

# Enhanced catalytic (ep)oxidation of olefins by VO(II), ZrO(II) and Zn(II)-imine complexes; extensive characterization supported by DFT studies



Mohamed Shaker S. Adam<sup>a,b,\*</sup>, Laila H. Abdel-Rahman<sup>a</sup>, Hanan El-Sayed Ahmed<sup>a</sup>, M.M. Makhlof<sup>c</sup>, Mona Alhasani<sup>d</sup>, Nashwa M. El-Metwaly<sup>d,e</sup>

<sup>a</sup> Chemistry Department, Faculty of Science, Sohag University, Sohag-82534, Egypt

<sup>b</sup> Department of Chemistry, College of Science, King Faisal University, P.O. Box 400, Al Ahsa 31982, Saudi Arabia

<sup>c</sup> Department of Sciences and Technology, Ranyah University College, Taif University, P.O. Box 11099, Taif 21944, Saudi Arabia

<sup>d</sup> Chemistry Department, Faculty of Applied Science, Umm Al-Qura University, Makkah, Saudi Arabia

<sup>e</sup> Chemistry Department, Faculty of Science, Mansoura University, Mansoura, Egypt

## ARTICLE INFO

### Article history:

Received 4 November 2020

Revised 27 February 2021

Accepted 11 March 2021

Available online 19 March 2021

### Keywords:

Imine complexes

Studies in solution

DFT

Catalytic (ep)oxidation; 1,2-cyclohexene  
2-aminothiophene

## ABSTRACT

Three mononuclear di-valent VO<sup>2+</sup>, ZrO<sup>2+</sup> and Zn<sup>2+</sup>-complexes (VOL, ZrOL and ZnL, respectively) were prepared from asymmetrical di-basic tetradentate di-imine ligand (6,6'-((1E,1'E)-(4-chloro-1,2-phenylene)bis(azaneylylidene))bis(methaneylylidene))bis(2-ethoxy phenol, H<sub>2</sub>L). To confirm the M-complexes compositions, various spectral tools (FT-IR, EI/M and UV-Vis. spectra), molar conductance, thermal, elemental analysis and pXRD analyses were accomplished. Distorted octahedral geometry was confirmed for ZnL and square pyramidal geometry was elucidated for VOL and ZrOL. Their catalytic efficiency was investigated in the epoxidation of 1,2-cyclohexene by H<sub>2</sub>O<sub>2</sub>. They exhibited moderate to excellent catalytic control. The effect of temperature, time, solvent, type of oxidant and amount of catalysts were studied in order to determine the optimal catalytic atmosphere. The catalysts screening for epoxidation of alternative cyclic and acyclic olefins at optimization was reported. The variation of central metal ions from high to low valents (Zr<sup>4+</sup>, V<sup>4+</sup> and Zn<sup>2+</sup> ions) and their capability for oxidation control their catalytic potential are the most effective aspects in the epoxidation reaction. The catalytic oxidation of 2-aminothiophene within VOL, ZrOL and ZnL, as a first trial, by H<sub>2</sub>O<sub>2</sub> was examined. Also, QSAR parameters and DFT studies were performed to predict the catalytic properties of VOL, ZrOL and ZnL, to assert on chosen application. Effective surface properties of VO(II) complex were promoted for progressing its catalytic activity, which already happened. The catalytic mechanism was supported by the sequenced stability difference between proposed intermediates based on the difference in their recorded formation energy from the DFT study.

© 2021 Elsevier B.V. All rights reserved.

## 1. Introduction

Imines are characterized by azo-methine moiety, in which the imino-group (C=N) could be formed within simple one-pot condensation of the substitutes C=O group of aldehyde or ketone with amines [1]. For more than a century, M-imine complexes gained a distinguished attentiveness by the inorganic chemists

due to their remarkable easy synthesis, high biological potential [2], variable catalytic performance [3], considerable electro-luminescent properties [4], remarkable fluorescence features [5], nonlinear optical properties (NLO) [6], applicable sensors [7] and organic photovoltaic material application [8]. According to their high tenability, most imines form high stable M-chelating complexes with most of the transition metals [9]. d-Block element complexes with imines as homogeneous [10] and heterogeneous [11] catalysts possess fascinating reactivity in various chemical organic syntheses [12]. Indeed, the epoxidation of C=C double bands of unsaturated hydrocarbons, which achieved catalytically by transition metal complex catalysts, is of interest in

\* Corresponding author.

E-mail addresses: [madam@kfu.edu.sa](mailto:madam@kfu.edu.sa), [shakeradam61@yahoo.com](mailto:shakeradam61@yahoo.com) (M.S.S. Adam), [m.makhlof@tu.edu.sa](mailto:m.makhlof@tu.edu.sa) (M.M. Makhlof), [n.elmetwaly00@yahoo.com](mailto:n.elmetwaly00@yahoo.com), [nmmohamed@uqu.edu.sa](mailto:nmmohamed@uqu.edu.sa) (N.M. El-Metwaly).

many transmetalations of organic substrates [10–12]. The produced epoxides of the epoxidation processes, which considered industrial intermediates, are highly applicable in the synthetic organic technology [10].

For that purpose, numerous reported works were promoted in the synthesis and catalytic epoxidation studies of alternative transition metal complex catalysts to reach the optimization with less required temperature and time [12]. Oxo and/or dioxo-vanadium (IV)/(V) imine complexes are appreciated as the most favored choice and the promising effective catalysts for such redox systems with different usable oxidants [13,14]. On the other hand, zinc (II)-complexes were not so the preferable catalysts in the oxidation of organic compounds, e.g. olefins, due to their high stable oxidation state [15]. However, the catalytic reactivity of zinc (II) complexes, as sufficient catalysts, was studied recently by Nunes et al. in the epoxidation of olefins using  $H_2O_2$  [16]. The immobilization of Mn(II)-salen complex on the modified alkoxy-ZnPS-PVPA considerably improved the catalytic potential of both Mn(III) and Zn(II) ions in the asymmetric epoxidation of olefins [17], in which  $Zn^{2+}$  ions improved the catalytic efficiency of the  $Mn^{2+}$ -complexes. Additionally, it is so far in the literature to report such catalytic susceptibility of oxo-zirconium complexes in the epoxidation of olefins. The high electrophilic character of  $Zr^{4+}$  ion in its reagents motivated its catalytic reactivity toward organic syntheses, such as  $ZrCl_4$  [18]. The catalytic ring-opening polymerization of lactide was assessed by  $Zr^{4+}$ -complex of phosphasalen [19], by  $Zr^{4+}$ -amino-benzotriazole phenolate complexes [20] and by some Zr-salen complexes [21], affording high potentiation. This could encourage us here to investigate the catalytic potential of a new oxo-zirconium complex, as a homogeneous catalyst in some epoxidation protocols. The strong Lewis acidity and the high valent of  $V^{4+/5+}$  ions in their complex catalysts could promote remarkably their catalytic potential over those catalysts of very high stable low valent metal ions, i.e.  $Zn^{2+}$ -catalysts [22]. As well documented, the most favorable oxidizing agent, as a green reagent, is  $H_2O_2$ . It is classified as a safely stored, high effective, cheap oxygen source and highly environmentally attractive because of the green by-products of its oxidation processes, oxygen and water [23].

The coordinated ligands as the organic backbone show a respectable influence in the catalytic activity of their metal complexes [24]. The chelating, electronic and steric effects of the coordinated ligand are of interest in the measuring of the M-complexes reactivity in catalysis [25]. This could be beneficial here to present the role of the coordinated imine ligand in the catalytic epoxidation of olefins with various metal ions.

Although, the high applicability of 2-aminothiophene in biological and industrial proposes [26], its catalytic oxidation was not yet reported in the literature. Depending on those efforts, we report here the preparation of three imine complexes from 6,6'-((1E,1'E)-((4-chloro-1,2-phenylene)bis(azaneylylidene))bis(methaneylylidene))bis(2-ethoxyphenol) with different metal ions ( $ZrO^{2+}$ ,  $VO^{2+}$  and  $Zn^{2+}$  ions) with achievement of their physicochemical characteristics. The catalytic evaluation of the three M-imine complexes was examined here in redox processes of some unsaturated hydrocarbons. The effect of the oxidation state of the central metal ion ( $ZrO^{2+}$ ,  $VO^{2+}$  and  $Zn^{2+}$  ions) was also evaluated, comparatively. Various parameters (temperature, time, oxidant and solvent) were studied to get the optimization of the catalytic reactions. Interestingly, we present all possible products of 2-aminothiophene oxidation catalyzed by the current M-complexes. Computerized studies were done to prove the steric-structures as well as to develop theoretical controls for the catalytic behavior and confirm the previously proposed mechanism.

## 2. Experimental

### 2.1. Chemicals and Solvents

The involving starting materials, reagents and organic solvents, which benefit in the syntheses and catalytic studies are commercially available with high purity form without specific purification (Sigma Aldrich, Acros, Fluka and Merck).

### 2.2. Physical methods

$^1H$  and  $^{13}C$  NMR spectra of  $H_2L$  and  $ZrOL$  were scanned by utilizing a Bruker Advance DPX-500 spectrometer. pXRD powder, UV-Visible, FT-IR, mass spectra and CHN analyses of the studied compounds were determined by Bruker D8 Advance, UV-Vis spectrophotometer Q5000, a Shimadzu FTIR-8300 spectrophotometer, DI analysis Shimadzu Qp-2010 plus and a PerkinElmer 240c elemental analyzer, respectively. Thermogravimetric analysis was conducted with a heating rate of  $10^\circ C \text{ min}^{-1}$  with DTG 60H Detector. Magnetic and conductivity measurement was measured utilizing a Gouy balance and a Jenway 4510 conductivity meter, respectively.

### 2.3. Preparation of $H_2L$ ligand and its M-complexes

Depending on the previous synthesis of the current  $H_2L$  ligand [27], 6,6'-((1E,1'E)-((4-chloro-1,2-phenylene)bis(azaneylylidene))bis(methaneylylidene))bis(2-ethoxyphenol) ( $H_2L$ ) ligand was prepared by heating an ethanol solution (20 mL) of 4-chloro-o-phenylenediamine (0.71 g, 5.0 mmol) with an ethanol solution (20 mL) of 3-ethoxy-salicylaldehyde (1.66 g, 10 mmol) for 2 h at  $70^\circ C$ . The resulting deep orange solid was filtered, washed with ether and recrystallized in ethanol.

The obtained  $H_2L$  ligand (deep orange) gave yield 85% with m.p.  $200^\circ C$ . FT-IR (KBr,  $cm^{-1}$ ): 1612 (C=N), 3423 (–OH).  $^1H$  NMR (DMSO- $d_6$ ,  $\delta$ , ppm): 12.78–12.71 (s, 2H, 2OH), 8.96 and 8.91 (s, 2H, 2CH=N), 7.60–6.89 (m, 9H, 9CHar), 4.10–4.04 (q,  $^4J = 1.8 \text{ Hz}$ ,  $^3J = 5.9 \text{ Hz}$ , 4H, 2OCH<sub>2</sub>), 1.38–1.33 (t,  $^3J = 5.4 \text{ Hz}$ , 6H, 2CH<sub>3</sub>).  $^{13}C$  NMR (DMSO- $d_6$ ,  $\delta$ , ppm): 15.00 (CH<sub>3</sub>), 15.23(CH<sub>3</sub>), 64.32(CH<sub>2</sub>), 64.62 (CH<sub>2</sub>), 112.97 (CH), 116.29 (CH), 118.44 (CH), 119.16 (CH), 119.33(CH), 119.46 (CH), 119.75 (CH), 121.17 (CH), 122.94 (CH), 123.55 (CH), 146.42 (CH), 146.99 (CH), 147.50 (C<sub>q</sub>), 147.91 (C<sub>q</sub>), 148.20 (C<sub>q</sub>), 149.07 (C<sub>q</sub>), 151.39 (C<sub>q</sub>), 153.61 (C<sub>q</sub>), 193.06 (CH, 2CH=N). Anal. Calc. for  $C_{24}H_{23}ClO_4N_2$  (%): N, 6.38; C, 65.60; H, 5.23, found (%): N, 6.30; C, 65.70; H, 5.30.

A facile preparation method was employed for metal complexation within mixing of an equimolar ratio (3.0 mmol) of  $H_2L$  (1.32 g, 5 mmol) in ethanol (20 mL) with  $H_2O/EtOH$  solution (20 mL) of 5 mmol of  $ZrOCl_2 \cdot 8H_2O$  (0.97 g),  $VO(acac)_2$  (0.79 g) or  $Zn(acac)_2 \cdot 2H_2O$  (0.66 g) with heating for at  $70^\circ C$  2 h. The resulting precipitate was filtered, washed with ether and recrystallized in ethanol. The purity of prepared complexes was monitored by TLC.

The obtained  $ZrOL$  complex (orange) gave yield 74% with m.p.  $< 300^\circ C$ . FT-IR (KBr,  $cm^{-1}$ ): 1608 (C=N), 434 (M–N), 504 (M–O). Anal. Calc. for  $C_{24}H_{25}ClN_2O_7Zr$  (%): N, 4.83; C, 49.66; H, 4.31, found (%): N, 4.90; C, 49.74; H, 4.22.  $\mu_{eff}$  (B.M.): diamagnetic.  $^1H$  NMR (DMSO- $d_6$ ,  $\delta$ , ppm): 9.53 and 9.27 (s, 2H, 2CH=N), 7.84–7.46 (m, 9H, 9CHar), 4.88–4.51 (q,  $^4J = 1.3 \text{ Hz}$ ,  $^3J = 5.5 \text{ Hz}$ , 4H, 2OCH<sub>2</sub>), 1.58–1.42 (t,  $^3J = 5.1 \text{ Hz}$ , 6H, 2CH<sub>3</sub>).

The obtained VOL complex (olive-green) gave yield 70% with m.p.  $< 300^\circ C$ . FT-IR (KBr,  $cm^{-1}$ ): 1574 (C=N), 452 (M–N), 532 (M–O). Anal. Calc. for  $C_{24}H_{21}ClN_2O_5V$  (%): N, 5.55; C, 57.14; H, 4.16, found (%): N, 5.62; C, 57.06; H, 4.10.  $\mu_{eff}$  (B.M.): 1.76,  $\Lambda_m$ :  $3.9 \Omega^{-1} \text{ mol}^{-1} \text{ cm}^2$ .

The obtained ZnL complex (brown) gave yield 71% with m.p. < 300°C. FT-IR (KBr, cm<sup>-1</sup>): 1578 (C=N), 436 (M–N), 519 (M–O). Anal. Calc. for C<sub>24</sub>H<sub>29</sub>ClN<sub>2</sub>O<sub>8</sub>Zn (%): N, 4.87; C, 50.17; H, 5.05, found (%): N, 4.80; C, 50.25; H, 5.12.  $\mu_{\text{eff}}$  (B.M.): diamagnetic.

#### 2.4. Kinetic and thermodynamic parameters

The thermal decomposition of the studied M-chelates was examined kinetically by applying Coats–Redfern relation, as shown in Eq. 1 [28]:

$$\log \left[ \frac{\log (w_{\infty} / (w_{\infty} - w))}{T^2} \right] = \log \left[ \frac{RA}{E^{\neq} \phi} \left( 1 - \frac{2RT}{E^{\neq}} \right) \right] - \frac{E^{\neq}}{2.303R T} \quad (1)$$

where, W and W<sub>∞</sub> are the mass loss at a defined temperature T of the studied compounds and the mass loss after their complete decomposition, respectively. R and φ are the general constant of gases and the heating rate, respectively. The graph was plotted from the left side of Eq. 1 against 1/T, since  $\left(\frac{2RT}{E^{\neq}}\right) \approx 0$ . Moreover, the kinetic parameters namely frequency factor (A) and activation energy (E<sup>≠</sup>) were calculated from the intercept and the slope, respectively. The thermodynamic parameters of the activation enthalpy, ΔH, and the activation entropy, ΔS, were determined from the activation energy, E<sup>≠</sup>, using the well knowing Arrhenius relations [29].

#### 2.5. Studies in solution

The VO, ZrO- and Zn-complexes stoichiometry was studied in the solution using continuous variation (Jobs method) and molar ratio methods [28]. Sequenced alternating changes in concentrations between metal and ligand solutions (1 × 10<sup>-2</sup> mol dm<sup>-3</sup> in DMF) were kept in balance for 2 h. Then, the absorbance was recorded at λ<sub>max</sub> for each solution of corresponded M-complex. The plot was drawn between absorbance and mole fraction of ligand for each M-complex. The forming constants (K<sub>f</sub>) of M-complexes were gained by utilizing continuous variation curves according to Eq. 2:

$$K_f = \frac{\left(\frac{A}{A_m}\right)}{\left(1 - \left(\frac{A}{A_m}\right)^2\right) C} \quad (2)$$

where, A and A<sub>m</sub> are arbitrarily chosen from absorbance values either a part from absorbance peak or maximum absorbance, respectively and C is the primary molar concentration of metal ion solution. Also, Gibb's free energy of each M-complex (ΔG<sup>≠</sup>) was calculated from this equation: ΔG<sup>≠</sup> = -RTlnK<sub>f</sub>.

#### 2.6. Catalytic procedures

In a round glass flask (100 mL) with two-neck (connected with a capacity of 100 mL, equipped with fitted glass water circulated condenser), the 1,2-cyclohexene epoxidation or the 2-aminothiophene oxidation was accomplished within (0.02 mmol) M-complex catalyst (VOL, ZrOL or ZnL) in 10mL acetonitrile (standard solvent or other used solvents), homogeneously, at various reaction temperature (from 50 to 100°C) with continuous stirring at the given time. Each catalytic reaction was started by adding the oxidant (3.0 mmol of 30% H<sub>2</sub>O<sub>2</sub>, 1.7 mmol of 70% tBuOOH or 1.7 mmol of solid NaClO<sub>4</sub>) to the reaction solution. The progress of the reaction was monitored kinetically by withdrawing ~ 10.0 μL from reaction contents. The taken samples were mixed with solid MnO<sub>2</sub> (0.2 g) destroying the excess amounts of H<sub>2</sub>O<sub>2</sub> or tBuOOH and also with anhydrous CaCl<sub>2</sub> to absorb water from treated samples. Then, the resulted samples were filtrated through 0.3 g celite and then

diluted with acetonitrile. The obtained sample (1 μL) was delivered to the GC/MS apparatus. The chemoselective products were determined with retention time and also compared with those of authentic stored compounds. For the catalytic reaction in water, the obtained products were extracted using Et<sub>2</sub>O (diethyl ether).

The yield percentages of desired products of epoxy-1,2-cyclohexane for the 1,2-cyclohexene epoxidation were monitored by GC/MS, Shimadzu (Gas Chromatography mass spectrometer) of QP2010 SE model with Rxi-5 Sil mass spectroscopy. The characterization of the capillary column was considered as 0.25 mm ID × 30 m length × 0.25 um film thickness. The withdrawing samples were injected into the GC/MS within an auto-sampler. The temperature of the provided oven was kept at 40°C for 1 min. The oven temperature was increased with a rate of 10°C per 1 min to 200°C. At 200°C, the inlet process was operated with the splitless mode of the transfer line. The carrier gas was He (Helium) with a purity of 99.999%. Its flow rate was carried out with 1 mL per 1 min. The high-performance quadrupole mass filter and Shimadzu's proprietary Optdesign simulation program with high-quality mass spectra were supplied. EI is the ionization method for the molecular weight information. EI with selectively measuring, high sensitivity, chemical substances and an electron affinity were used in the GC-MS. The Lab solution software was used to emphasize the amount of product yield percentage for each sample from the desired products.

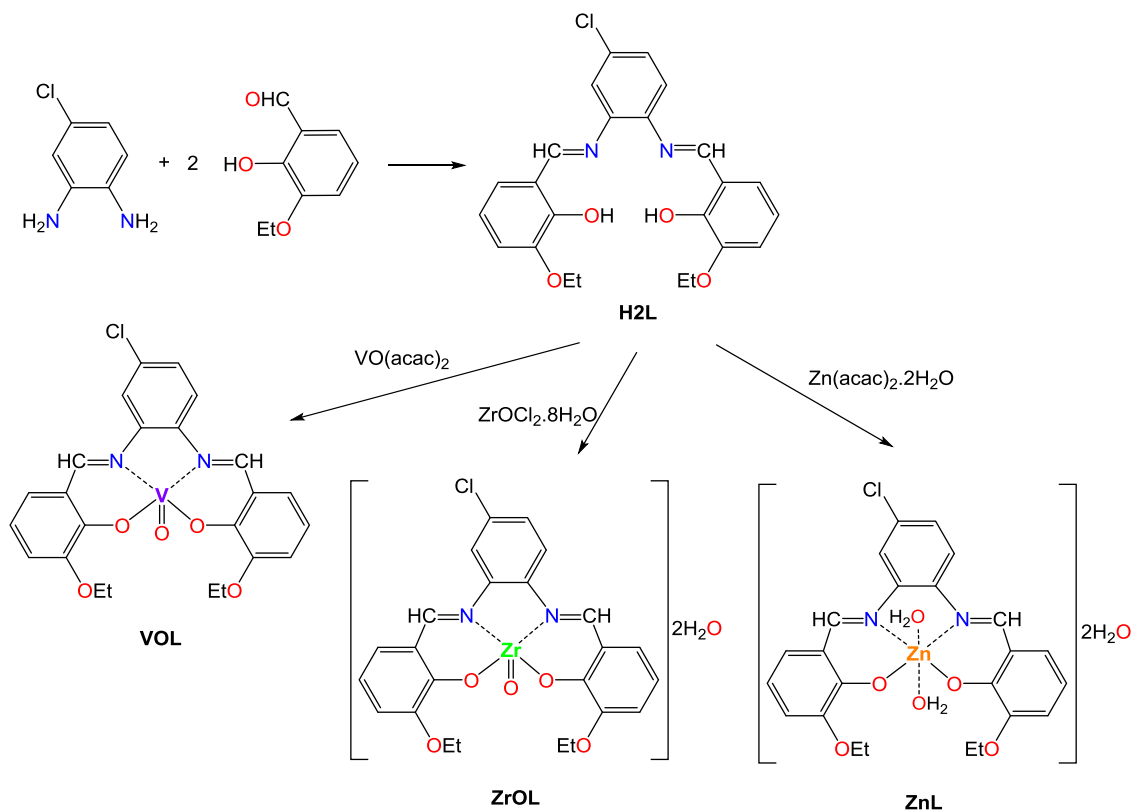
#### 2.7. Computational study

All computations were accomplished using the Gaussian09W software package [30]. The geometry of studied compounds was fully optimized using DFT/B3LYP method [31] without symmetry constraints. Using Becke3–Lee–Yang–Parr (B3LYP) exchange-correlation functional under 6-311G<sup>++</sup> basis set. The suitability of final optimized forms was confirmed by positive values of frequency calculated. The time-dependent DFT (TD-DFT) was conducted by utilizing the polarizable continuum model by applying an integral equation formalism variant (IEF-PCM) at the same B3LYP level, to study properties of the ground and excited states [32]. All computational files (log, chk and fchk) were visualized over Gauss-View version 5.0.9 [33] to extract all displayed features. Among that, the optimized structures, frontier orbitals and electrostatic potential maps that built over new cubic contours. Moreover, essential physical parameters were calculated by using so easy method [34].

### 3. Results and discussion

#### 3.1. Practical characterization for synthesizes

The synthesis of the current H<sub>2</sub>L ligand was already reported elsewhere [27], whereas the VO-, Zn- and ZrO-complexes are the subject presented in this work. They are characterized by alternative spectral tools, NMR, IR, MS and UV-Vis., as well as, EA (micro-analysis), TGA (thermogravimetric analyses) and magnetic features. Synthesis VOL complex was already reported with studying its biological reactivity elsewhere [27]. The free ligand H<sub>2</sub>L and its solid complexes (ZnL, ZrOL and VOL) are highly stable in air and moisture (Table 1) for a long time. The obtained results of molecular formula, melting/decomposition points, molar conductivity, magnetic moment measurements and elemental analysis are registered (Table 1). ZnL, ZrOL and VOL are intensely amorphous colored material and decomposes above 300°C. The stoichiometry results indicated that H<sub>2</sub>L behaves as a dibasic tetra-dentate ligand and coordinates with the metals ions through 1: 1 (M: L) stoichiometry (Scheme 1).



**Scheme 1.** Preparation strategy for the H<sub>2</sub>L ligand and its VO-, ZrO- and Zn-complexes.

### 3.1.1. Microanalysis, magnetic and conductivity features

The obtained elemental CHN analyses of the studied compounds are agreed with the calculated ones for their experimental formula, which suggests 1: 1 molar ratio based on bibasic tetradentate ligand with each metal ion. Magnetic measurements of complexes agree with a d<sup>0</sup> electronic configuration of ZrOL and ZnL complexes that have a square pyramidal and octahedral geometries, respectively. VOL complex is paramagnetic (1.76 B.M.) with d<sup>1</sup> electronic configuration and has square pyramidal geometry [13]. Molar conductance of M(II)-complexes ( $1 \times 10^{-3}$  M in DMF) reveals low values ( $1.9\text{--}8.0 \Omega^{-1}\text{cm}^2 \text{mol}^{-1}$ ), which indicating non-electrolytic features of them [35].

### 3.1.2. <sup>1</sup>H & <sup>13</sup>C-NMR spectra of the ligand

The <sup>1</sup>H-NMR spectrum of H<sub>2</sub>L ligand exhibits singlet signals at 12.78 and 12.71 ppm for two hydroxyl protons, which disappeared when D<sub>2</sub>O was added to its deuterated solution (Fig. S1a). For the <sup>1</sup>H-NMR spectra of ZrOL complex, the two distinguished OH-proton signals are completely disappeared. The two hydroxy groups coordinated to ZrO<sup>2+</sup> ion within the negative charge of the deprotonated group. Two azo-methine protons offer two singlet peaks at 8.96 and 8.91 ppm and the aromatic protons present multiple signals in the area from 7.60 to 6.89 ppm for H<sub>2</sub>L. Both signals for the two azo-methine protons were strongly shifted to be located at 9.53 and 9.27 ppm, referring to their coordination to ZrO<sup>2+</sup> ion through the nitrogen lone pair of electrons, as observed elsewhere for similar Zr-chelating complexes [20]. Additionally, the two -OCH<sub>2</sub> groups show multiple signals at 4.10–4.04 ppm for H<sub>2</sub>L and at 4.88–4.51 ppm for ZrOL complex. The two -CH<sub>3</sub> chains of the ethoxyl groups display multiple signals at 1.38–1.33 ppm for H<sub>2</sub>L (Fig. S1a) and at 1.58–1.42 ppm for ZrOL complex. <sup>13</sup>C-NMR spectrum assigns signals in the aliphatic region for CH<sub>3</sub> carbon atoms at  $\delta$  15.00–15.23 ppm and -OCH<sub>2</sub> carbon atoms at 64.62–64.93 ppm. The carbon atoms assign <sup>13</sup>C-NMR signals at 112.97–153.61

ppm for the aryl rings and 193.06 ppm for the imino groups, as presented in Fig. S1b.

### 3.1.3. Comparative IR-vibrations

To distinguish the characteristic mode of bonding of the ligand and towards Zn<sup>2+</sup>, ZrO<sup>2+</sup> or VO<sup>2+</sup> ion to form the corresponded M-chelating complexes, the ligand's IR spectrum of its functional groups was compared to those of its M-complexes spectra. The characteristic IR frequencies of the prepared H<sub>2</sub>L ligand and its M-imine chelates are showed in Table 1 and displayed in Figs. S2a,b,c,d. A sharp strong band of the azo-methine groups appears at 1612 cm<sup>-1</sup> in the spectrum of the H<sub>2</sub>L ligand, in which its frequency was decreased (1608, 1578 and 1579 cm<sup>-1</sup>) after complexation with ZrO<sup>2+</sup>, VO<sup>2+</sup> and Zn<sup>2+</sup> ions, respectively. This indicates the two azo-methine coordination through the two nitrogen atoms in the complex formation [36]. Also and regarding the M-complexes spectra, obscure of broad weak  $\bar{\nu}_{\text{OH}}$  band, which appeared for the H<sub>2</sub>L ligand's spectrum (3423 cm<sup>-1</sup>), indicates the participation of two ionized deprotonated hydroxyl groups to ZrO<sup>2+</sup>, VO<sup>2+</sup> and Zn<sup>2+</sup> ions [36]. This proposed a dibasic tetradentate mode of bonding for imine ligand within all M-complexes. Remarkably, the water molecules reveal  $\rho_{\text{r}}(\text{H}_2\text{O})$  and  $\rho_{\text{w}}(\text{H}_2\text{O})$  bands at 854.61 and 738.39 cm<sup>-1</sup>, respectively, besides,  $\bar{\nu}_{\text{OH}}$  3315 cm<sup>-1</sup> in ZrOL spectrum [37]. In ZnL complex, such bands were appeared at 823.88, 734.7 and 3418 cm<sup>-1</sup>, sequentially. New bands that appeared at the lower wavenumber region (532–504 cm<sup>-1</sup>) were assigned for  $\bar{\nu}_{\text{(M-O)}}$  and  $\bar{\nu}_{\text{(M-N)}}$  vibrations and confirm coordinating NO donors (Table 1) [13]. The phenolic  $\bar{\nu}_{\text{(C-O)}}$  band, which appeared at 1080 cm<sup>-1</sup>, was shifted to the higher frequency at 1082, 1087 and 1094 cm<sup>-1</sup> in ZrOL, VOL and ZnL spectra, respectively, due to coordination after its ionization. Moreover,  $\bar{\nu}_{\text{(V=O)}}$  and  $\bar{\nu}_{\text{(Zr=O)}}$  bands appeared at 979 and 995 cm<sup>-1</sup> in their corresponding spectra, indicate their vibrational mode in square-pyramidal geometry [13].

**Table 1**  
Analytical, some IR bands, formation constants ( $K_f$ ), stability constant (pK) and Gibbs free energy ( $\Delta G^\circ$ ) of ligand and its complexes

Comp.	Color	Empirical formula; MW	m.p. (°C)	$\Delta_m(\Omega^{-1} \text{cm}^{-2} \text{Mol}^{-1})$	$\mu_{\text{eff}}$ (BM)	Analysis (%) Found (calc.)			$\nu_{(\text{C}=\text{N})}$	$\nu_{(\text{M}=\text{O})}$	$\nu_{(\text{M}=\text{N})}$	$K_f \times 10^5$	pK	$\Delta G^\circ$ (KJ mol $^{-1}$ )
						C	H	N						
H <sub>2</sub> L	deep orange	C <sub>24</sub> H <sub>23</sub> ClN <sub>7</sub> O <sub>4</sub>	200	—	—	65.70 (65.60)	5.30 (5.23)	6.30 (6.38)	1612	—	—	—	—	—
[ZrO(L)] <sub>2</sub> ·2H <sub>2</sub> O; ZrOL	Orange	C <sub>24</sub> H <sub>25</sub> ClN <sub>7</sub> O <sub>7</sub> Zr	< 300	1.9	—	49.74 (49.66)	4.22 (4.31)	4.90 (4.83)	1609	504	434	5.9	-5.77	-32.92
[VO(L)]; VOL	Olive green	C <sub>24</sub> H <sub>21</sub> ClN <sub>7</sub> O <sub>5</sub> V	< 300	3.9	1.76	57.06 (57.14)	4.10 (4.16)	5.62 (5.55)	1603	532	452	6.5	-5.81	-33.16
[Zn(L)(H <sub>2</sub> O) <sub>2</sub> ] <sub>2</sub> ·2H <sub>2</sub> O; ZnL	Brown	C <sub>24</sub> H <sub>29</sub> ClN <sub>7</sub> O <sub>8</sub> Zn	< 300	8.0	—	50.25 (50.17)	5.12 (5.05)	4.80 (4.87)	1610	519	436	5.0	-5.69	-32.51

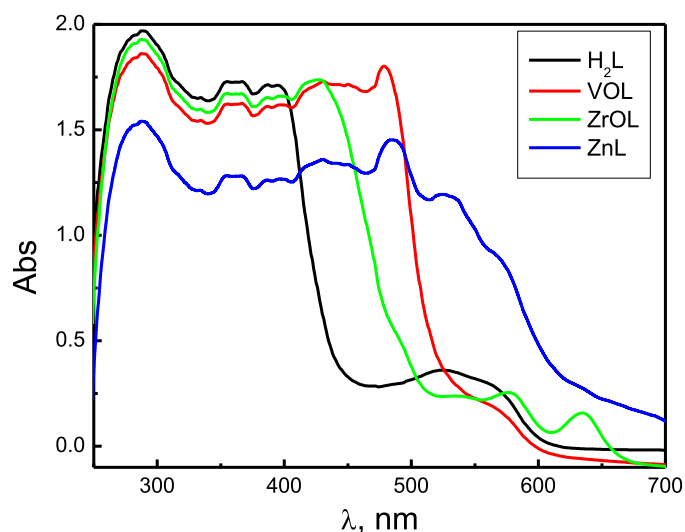


**Fig. 1.** UV-Vis spectra of the ligand H<sub>2</sub>L, ZrOL, VOL and ZnL complexes dissolved in methanol with  $\sim 1 \times 10^{-5}$  M at the wavelength range 200–800 nm at ambient temperature.

### 3.1.4. UV-Vis spectra and optical band gap

UV-Vis spectra are the most effective technique implemented to study the structural forms of the tested transition metal complexes [37]. The concentration  $1 \times 10^{-3}$  M was prepared from each compound in methanol and scanned over 200–800 nm range, at room temperature. Molar absorptivity ( $\epsilon_{\text{max}}$ ) and the maximum of absorption peaks ( $\lambda_{\text{max}}$ ), were obtained from UV-Vis spectra (Fig. 1) and tabulated in Table S1. The ligand spectrum displayed  $\pi \rightarrow \pi^*$  and  $n \rightarrow \pi^*$  transitions, which suffer shift due to the coordination of azomethine and enolized hydroxyl groups. Remarkable charge transfer bands ( $L \rightarrow M$ ) were recorded at 636, 479 and 524 nm in ZrOL, VOL and ZnL complexes, respectively. This feature is the main cause for the color depicted on such a diamagnetic octahedral complex. Moreover, VOL spectrum displayed a  $d \rightarrow d$  transition band at 570 nm that attributes to  ${}^2B_2 \rightarrow {}^2B_1$  transition in square-pyramidal geometry. Also, square-pyramidal geometry was proposed for ZrOL complex, as the favorable configuration for oxy-metals of the  $d^0$  system.

The optical band gap ( $E_g$ ) measures the magnitude of separation between the ground and excited states under influence of UV-Vis spectra. Consequently,  $E_g$  value is the lowest photon energy needed to release an electron from the ground to an excited state and leave a positive hole through the attraction force. Therefore, a reduced band gap denotes the near the conduction with the optical band and the excitation is carried out at low energy. Elastic electronic transition is preferable in different fields, as semiconductors-like and catalytic proposes [38]. The role of catalyst in the reaction is mainly focused on lowering the required activation energy as the preliminary step in the catalytic cycle. Also, the energy of 3d orbitals, which found in three metal ions, have a great impact on the activation energy and the catalytic efficiency. The values of  $E_g$  could be estimated from these relations Eqs. 3 and (4);

$$\alpha = 1/d \ln A \quad (3)$$

where,  $d$  is the width of the cell.

$$\alpha h\nu = A(h\nu - E_g)^m \quad (4)$$

where,  $\alpha$  is the absorption coefficient factor and  $A$  is a constant independent of energy. The values of  $m$  are 0.5 or 2, which attributed to the direct or indirect transition, respectively. The values of the absorption coefficient factor ( $\alpha$ ) were gained from Eq. 1 and used to calculated  $(\alpha h\nu)^2$ . A relation between  $(\alpha h\nu)^2$  and  $h\nu$

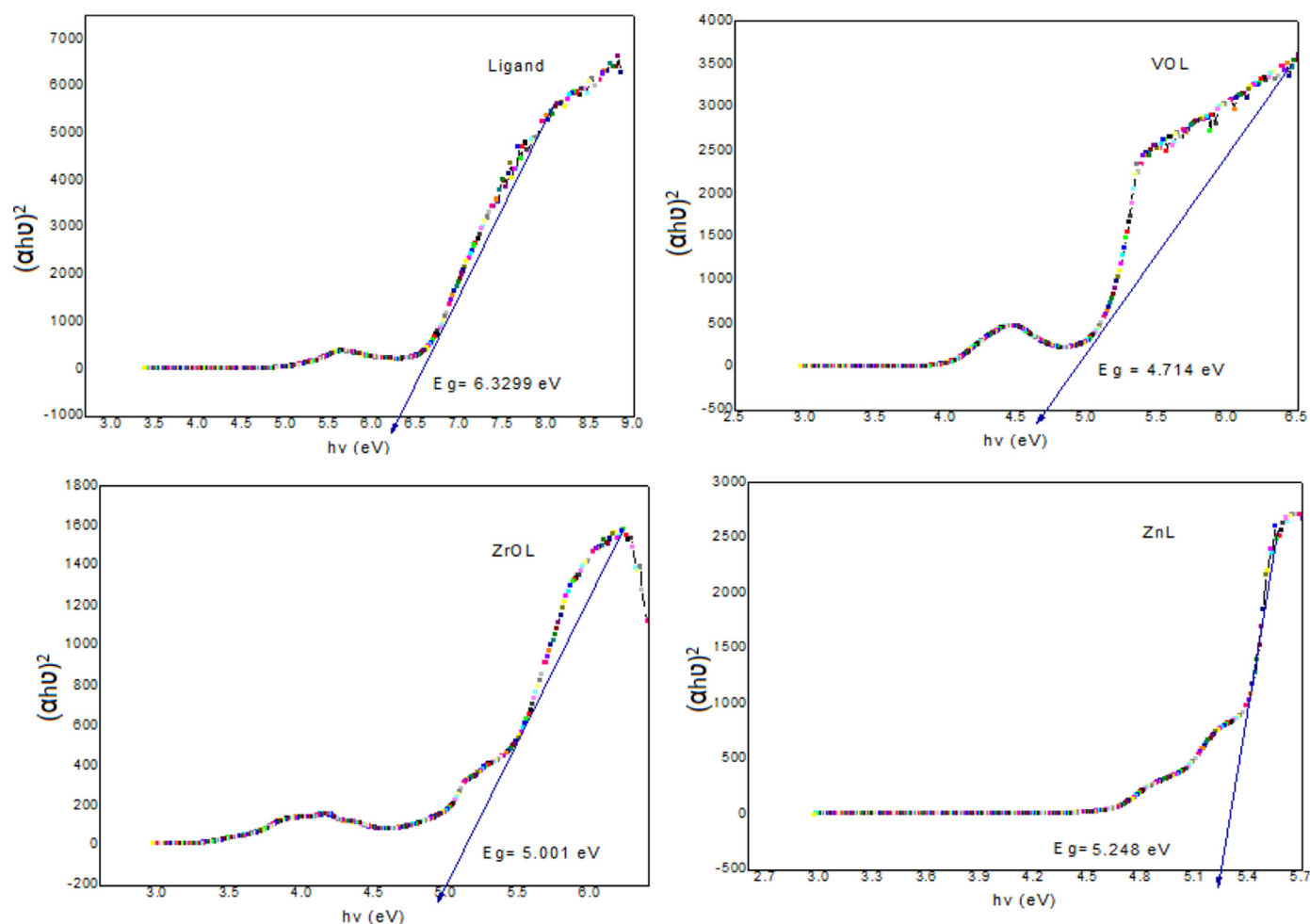


Fig. 2. Optical band gap for H<sub>2</sub>L ligand and its VO-, ZrO- and Zn-complexes.

(Fig. 2) was drawn, a line was extrapolated to interact x-axis in which  $(\alpha h\nu)^2 = 0$ , this point is the  $E_g$  value. The calculated values of the three complexes were appeared close to each other's, while lower than that of their free ligand (H<sub>2</sub>L). This refers to the closest optical properties of the three current complexes. So, we couldn't differentiate between them in their catalytic feature, but we expect a slight priority of VOL due to its  $E_g$  value affording the lowest one [39].

### 3.1.5. TGA and kinetic studies

Thermal analysis is widely used to study the thermophysical and kinetic properties of the M-complexes. Thermograms have been executed from 25 to 750°C under nitrogen and heating rate of 10°C/min, the decomposed mass verify molecular formulae suggested (Fig. S3).

TGA of ZrOL chelate shows lower thermal stability and full degradation reveals four steps. The first one starts at 38°C in agreement with the presence of two hydrated water molecules by 6.3% mass loss (calc. 6.3%). The second one at 150–300°C range attributes to the removal of C<sub>8</sub>H<sub>8</sub>O<sub>2</sub> with 23.4% mass loss (calc. 23.5%). The third stage at 300–450°C range refers to the C<sub>8</sub>H<sub>8</sub>O<sub>2</sub> removal with 23.5% mass loss (calc. 23.4%). The fourth stage at 450–730°C range assigns to the C<sub>8</sub>H<sub>5</sub>N<sub>2</sub>Cl loss with 28.4% mass loss (calc. 28.3%) leaving behind ZrO. TGA of VOL complex shows three degradation steps starting at 150°C, which indicates the lack of water presence with a loss of C<sub>8</sub>H<sub>8</sub>O<sub>2</sub> by mass loss of 26.9% (calc. 27.1%). The second step at 240–465°C range displays the removal of C<sub>8</sub>H<sub>8</sub>O<sub>2</sub> with 27.1% mass loss (calc. 27.0%). The third stage

at 465–740°C range refers to the C<sub>8</sub>H<sub>5</sub>N<sub>2</sub>Cl loss with 32.5% (calc. 32.6%) leaving behind VO species. The thermogram of ZnL complex presents lower thermal stability and full degradation reveals five steps. The first and second steps located at 25–110 and 110–230°C ranges, respectively, corresponded to the loss of two hydrated and two coordinated water molecules with 6.3% (calc. 6.2%) mass loss, respectively. The third step is found at the 230–390°C range, which is attributed to the C<sub>8</sub>H<sub>8</sub>O<sub>2</sub> removal with a mass loss of 23.6% (calc. 23.7%). The fourth step is recorded at 390–545°C range, which displayed for the C<sub>8</sub>H<sub>8</sub>O moiety loss with 21.0% mass loss (calc. 20.9%). The last step is presented in the range 550–710°C, which considered for the removed C<sub>8</sub>H<sub>5</sub>N<sub>2</sub>Cl part of the complex with a mass loss of 28.5% (Calc. 28.6%). The residual is ZnO.

Using Coats-Redfern relation, kinetic and thermodynamic parameters as, frequency factor (A), the energy of activation ( $E^*$ ), enthalpy energy ( $\Delta H^*$ ), entropy change ( $\Delta S^*$ ) and free energy change ( $\Delta G^*$ ) were estimated from TGA curves [40] (Table S3a-c). The positive values of activation energy reflect that the degradation processes are endothermic. The negative values of entropy consider that the prepared M-complexes are more ordered than the reactant and the reaction is slow. In the activated state, the polarization of bonds and electronic transitions may cause a slow reaction rate [41]. The high positive values of Gibbs free energy ( $\Delta G^*$ ) reflect that the decomposition steps are nonspontaneous processes, where the free energy of the initial compound is lower than that of the final residue. The low values of A implied a slow rate of pyrolysis. The great positive values of  $E^*$  indicate the presence of rotational, translational and vibrational states,

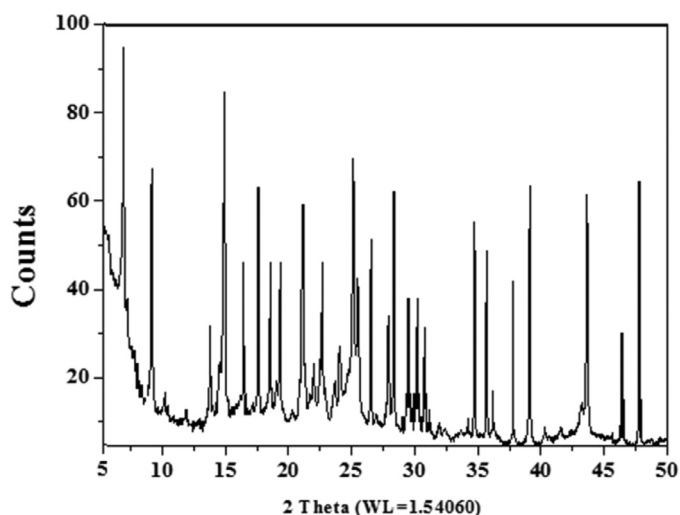


Fig. 3. Powder X-ray diffraction (pXRD) of the VOL complex.

and the variable mechanical potential energies for the current M-complexes.

### 3.1.6. Mass spectra of metal complexes

Mass spectra were accomplished for the studied VO-, ZrO- and Zn-complexes at 250°C and 70 eV within the electron ionization mode. Consequently, the resulted molecular ion peaks,  $[M^+]$  were displayed at  $m/z = 544$  (for ZrOL),  $m/z = 505/503$  (for VOL) and  $m/z = 579$  a. m. u. (for ZnL). The obtained mass spectra ensure the chemical structure of the current M-complexes, as shown in Figs. S5a,c,b, for VOL, ZrOL and ZnL, respectively. Besides, the peaks of metal isotopes were noticed in spectra at  $m/z = 50-90$  range.

### 3.1.7. Powder X-ray diffraction

Powder XRD patterns for  $H_2L$  ligand and its M-complex were taken over  $5^\circ < 2\theta < 60^\circ$  range using  $Cu/K\alpha$  radiation (1.54060 Å), as shown in Fig. 3 and Figs. S5a,b,c (in the supplementary materials). All patterns reflect relatively perfect nano-crystalline particles with polycrystalline or monoclinic nature where  $a \neq b \neq c$  and  $\alpha = \beta = 90 \neq \gamma$ . The pattern of  $H_2L$  ligand showed characteristic diffraction peaks with a maximum at  $2\theta = 24.8^\circ$ , which corresponded to inter-planar spacing (d) value of 3.58940 Å. The unit cell of  $H_2L$  ligand has lattice constants of  $a = 7.15800$ ,  $b = 30.88600$  and  $c = 7.37330$  Å with volume 1542 Å. pXRD pattern of VOL complex showed characteristic diffraction peaks with a maximum at  $2\theta = 6.9^\circ$ , which related to the d-spacing value of 13.4007 Å. The unit cell of the complex has lattice constants of  $a = 12.87200$ ,  $b = 7.61300$  and  $c = 20.69500$  Å with volume 2003.41 Å, as shown previously for other similar VO-complexes [42]. pXRD pattern of ZrOL complex showed characteristic diffraction peaks with a maximum at  $2\theta = 12.9^\circ$ , which exhibited a d-spacing value of 6.85380 Å. Unit cell of the complex has lattice constants of  $a = 15.56100$ ,  $b = 19.63600$ ,  $c = 13.77600$  Å with volume 4188.45 Å<sup>3</sup>. pXRD pattern of ZnL complex showed characteristic diffraction peaks with a maximum at  $2\theta = 6.2^\circ$ , which displayed a d-spacing value of 12.88640 Å. Unit cell of complex has lattice constants of  $a = 23.36500$ ,  $b = 12.74600$ ,  $c = 17.90400$  Å with volume 5224.71 Å<sup>3</sup>.

## 3.2. Studies in solution

### 3.2.1. Stoichiometry of complexes

Significant studies for M-chelating complexes in solution are completely different from those in solid-state. However, the stoichiometry of the formed complex in solution may agree with that

in the solid phase. Consequently, this study takes some importance to reflect a shadow on the credibility of complexes-stoichiometry in their solid-state. Using spectrophotometer to execute the continuous variation and the molar ratio routes for investigation in solution. The obtained relations (Figs. S6a,b) proposed 1: 1 ratio for the obtained complexes. This is due to the continuous variation curves offered maximum absorbance at a mole fraction of ligand  $X = 0.48-0.51$  and molar ratio curves assure 1: 1 ratio. The forming constants ( $K_f$ ) of complexes are recorded (Table 1) indicating high stability of 1: 1 ratio of the studied chelates. Moreover, the negative values of Gibb's free energy reflect the spontaneous feature of reactions [40].

### 3.2.2. Effect of pH on the M-complex stability

As seen, the dissociation curves for metal ion complexes in DMF (Fig. S7) indicate high stability of VO-, ZrO- and Zn-complexes over pH = 5-11 range. Therefore and regarding complex implementations, the appropriate pH range is wide enough for safe applications.

## 3.3. Catalytic epoxidation of 1,2-cyclohexene

Fundamentally, the catalytic efficiency of VO-, ZrO- and Zn-complexes was examined in the catalytic system of olefins epoxidation by a convenient oxidizing reagent under aerobic conditions. 1,2-cyclohexene is one of the most widespread standard examples of olefins for such systems.

Optimized homogeneous conditions for VOL, ZrOL and ZnL catalysts were estimated as a function of time at various temperatures, as reported previously [43]. Also, alternative reaction parameters, which could influence the selectivity and conversion, were studied. As reported, the percentages of conversion and selectivity of olefins epoxidation to corresponded epoxy-product, depend mainly on catalyst type, oxidant nature and reaction atmosphere (solvent, temperature and time) [12,44].

The catalytic reactions started by injection of 1,2-cyclohexene (1.0 mmol) by VOL, ZrOL or ZnL catalyst (0.02 mmol) and  $H_2O_2$  (3.0 mmol) (the oxidant) at different reaction temperatures in acetonitrile (10 mL). Various catalytic control and chemoselectivity for the conversion of 1,2-cyclohexene were shown in Tables S4-S6. The epoxidation process took place in a concerted one step with an explanation of the catalytic mechanistic pathway [45]. In the absence of a significant catalyst, there was no distinguished progress in the redox process even at high reaction temperatures.

### 3.3.1. Temperature Effect

At various temperatures, 50, 60, 70, 80, 90 or 100°C, the epoxidation reaction was investigated and percentages of the product yields were evaluated by GC/MS and listed (Tables S4-S6). At 50°C, a low temperature, the catalytic potential of all M-complexes was low even by prolongation of reaction time up to 6 h, as recorded in conversion and chemoselectivity percentages of the epoxy target (entries 1-4). The percentages of conversion were increased gradually with VOL (21, 34, 50 and 60%), ZrOL (9, 15, 28 and 40%) and ZnL (8, 13, 20 and 32%) during the running times, i.e. 1, 2, 4 to 6 h, respectively (Tables S4, S5 and S6). Considerably, the conversion percentages were enhanced gradually within the time for all catalysts with little reduction of the selectivity at 50°C (Fig. 6a-c).

Similarly, at 60°C, the yield percentages of the welcomed product were not highly promoted by time rising up to 6 h with all M-complexes. Remarkably, the yield percentages were promoted to 66, 62 and 64% within VOL catalyst after 6 h (entry 8, Table S4). Also, with ZrOL catalyst, the reaction afforded 53 % of the epoxy product. With ZnL catalyst, it affords 50 % from the selective product after 6 h. Hence, the TONs values were incremented gradually

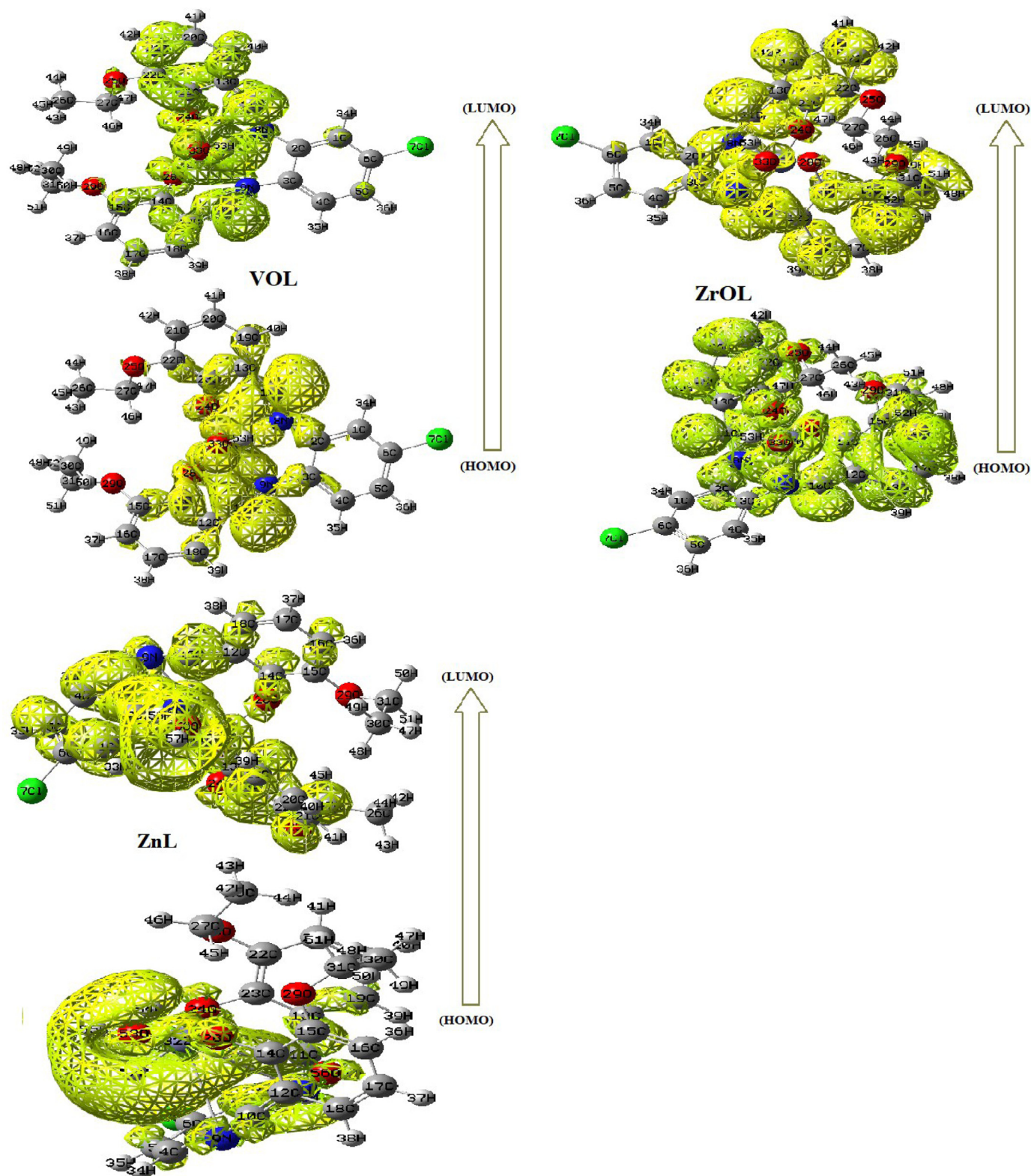


Fig. 4. Frontier orbitals for VO-, ZrO- and Zn-complexes.

with the lessening of TOFs values. Conclusively, the low temperatures, *i.e.* 50 and 60 °C, are not enough to progress such epoxidation protocols and to optimize the reaction conditions.

Particularly, at 70°C, the yield percentages, conversion and selectivity were increased to high percentages specifically after a long time (6 h). In the beginning, the amount of the epoxy prod-

uct was low to moderate after 1 h with all M-catalysts. The reaction showed 68, 38 and 36% with VOL, ZrOL and ZnL (entry 9, **Tables S4, S5 and S6**), respectively. The highest percentages were recorded after 6 h, as 87, 73 and 76% from epoxy-1,2-cyclohexane with VOL, ZrOL and ZnL (entry 12, **Tables S4, S5 and S6**), respectively.

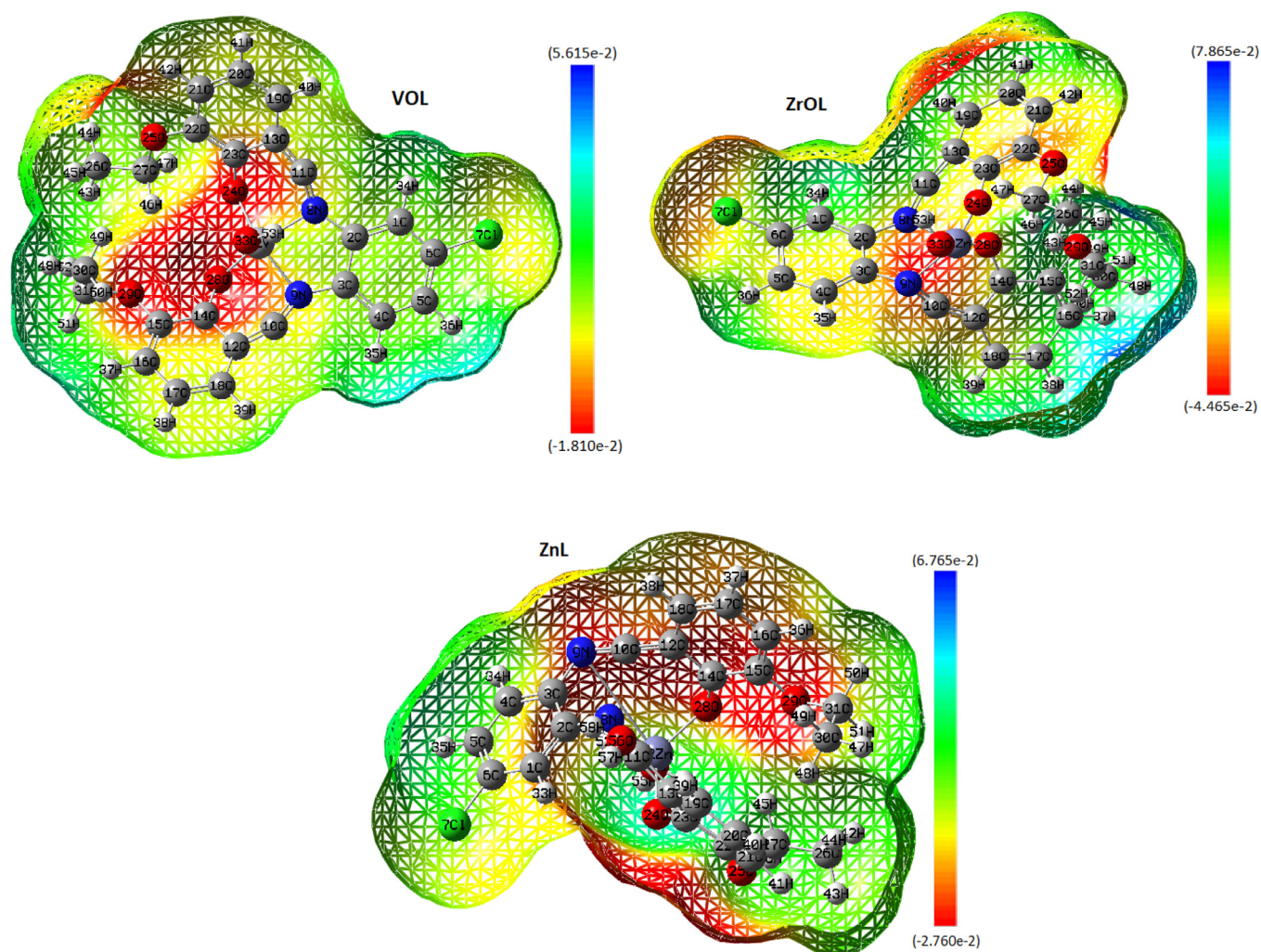


Fig. 5. Molecular electrostatic maps of VO-, ZrO- and Zn-complexes.

At the favored temperature in acetonitrile (80°C) for most reported epoxidation systems [46], ~100% was the recorded conversion for VOL, ZrOL and ZnL after 4 to 6 h (entries 15 and 16). Meanwhile, the selectivity was observed as the highest percentage after 1-2 h (entries 13 and 14, **Tables S4-S6**), and then it reduced by running time to 4-6 h (entries 15 and 16). After 1 h, the presented percentages were acceptable to be 81, 61 and 56% with VOL, ZrOL and ZnL (entry 10, **Tables S4, S5 and S6**), respectively. With 2 h, the yield percentages of the desired product was improved remarkably to be 87 (with VOL), 75 (with ZrOL) and 72% (with ZnL) (entry 14). Similarly and after 4 h, the yielding percentages of the welcomed product were also improved gradually as 90 (with VOL), 82 (with ZrOL) and 81% (with ZnL) (entry 15, **Tables S4-S6**). But, after 6 h, the catalytic system gave less product amounts with VOL (81%), ZrOL (82%) and ZnL (81%), as shown in **Fig. 6a-c**, entry 16.

Moreover, at 90°C more than the boiling point of acetonitrile, the conversion percentages increased fairly to 100% (entries 19 and 20) by the time. The selectivity was oppositely reduced notably after 1 h (93%, entry 17) up to 6 h (64%, entry 20) with VOL. Similar behavior was detected for ZrO-catalysts and Zn-catalysts (entries 17-20). The yield of the desired product was detected after 4 h with percentages of 84% with ZrOL (**Table S5**, entry 19), as shown from the TONs and TOFs values. For ZnL, the yield percentages were 86%, as reported in **Table S6**, entry 19.

At 100°C, a strong improvement in the yields of unwelcomed side products [11,12], which minimized the targeted yield of epoxy-1,2-cyclohexane (entries 21-24) with all M-catalysts, was neatly recorded. Also, excellent conversion and low selectivity percentages were observed at that temperature. Consequently, the evaporation of reaction components at 100°C, could take place and hence, could cause reducing in catalytic sufficiency. High temperature with an excess oxidant, could progress further oxidation of epoxy-1,2-cyclohexane in presence of M-catalysts to give other unwelcomed side products (see TONs and TOFs values, **Tables S4-S6**), as reported elsewhere [15].

Conclusively, catalytic reactivity of VOL, ZrOL and ZnL was promoted remarkably as a function of reaction temperature, **Fig. 6a-c**. In which, the best temperature depends on the percentages of conversion, selectivity and yield [10,15] and is considered as one of the optimized conditions. Here, VOL showed the optimal temperature at 80°C with 90% yield from the selective product after 3 h (entry 15, **Table S4**). On the other hand, ZrOL afforded the optimal temperature after 4 h, with 84 % of the target product at 90°C (entry 19, **Table S5**). Similarly, the reactions catalyzed by ZnL, awarded the best yield from the targeted product at 90°C after 4 h (86%), with very good selectivity (88%), (entry 19, **Table S6**). Finally, the catalyzed reactions with all M-complexes could be progressed with reaction temperatures from 70 to 90°C, referring to the high stability of complex catalysts in reaction media.

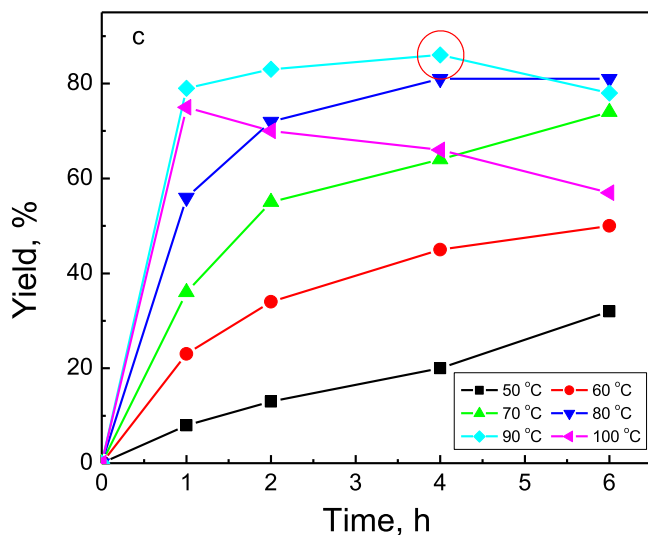
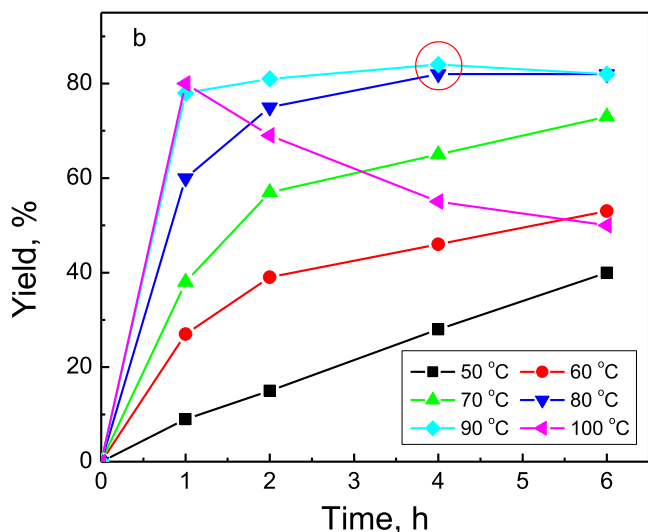
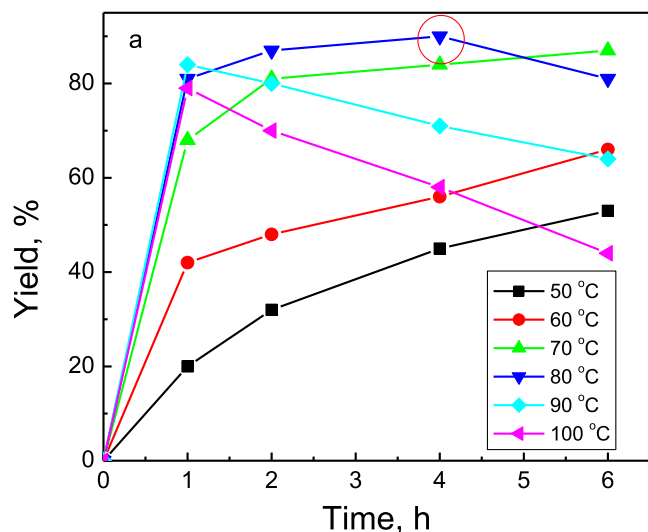


**Fig. 6.** The yield percentages of epoxy-1,2-cyclohexene of the epoxidation of 1,2-cyclohexene by  $\text{H}_2\text{O}_2$  catalyzed by (a) VOL, (b) ZrOL and (c) ZnL.

**Table 2**  
Solvent type effect on epoxidation of 1,2-cyclohexene by  $\text{H}_2\text{O}_2$ .

Catalyst <sup>a</sup>	Solvent	Yield (%) <sup>b</sup>			Conversion (%)	Selectivity (%)
		R	P	Side products		
VOL	AN	0	90	10	100	90
	EtOH	1	83	16	99	84
	$\text{H}_2\text{O}$	22	50	28	78	64
	DMSO	0	60	40	100	60
ZrOL	$\text{CHCl}_3$	0	81	19	100	81
	AN	0	84	16	100	84
	EtOH	11	57	32	89	64
	$\text{H}_2\text{O}$	27	41	32	73	56
ZnL	DMSO	2	58	40	98	59
	$\text{CHCl}_3$	0	72	28	100	72
	AN	6	85	9	94	90
	EtOH	10	70	20	90	78
	$\text{H}_2\text{O}$	27	44	29	73	60
	DMSO	0	67	33	100	67
	$\text{CHCl}_3$	0	77	23	100	77

<sup>a</sup> The epoxidation of 1,2-cyclohexene (R) (1.0 mmol) by an aqueous  $\text{H}_2\text{O}_2$  (3.00 mmol), catalyst (0.02 mmol) in 10 mL solvent at the optimized reaction time and temperature.

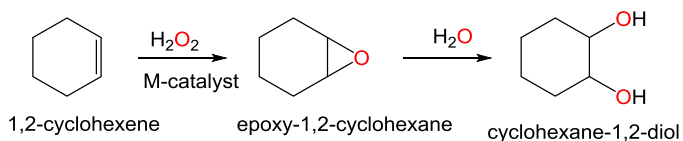
<sup>b</sup> The percentages derived from GC results, selectivity control of P, epoxy-1,2-cyclohexane, and the other side products.

### 3.3.2. Time Effect

The effect of time was considered in Figs. 6a-c, which present plotting of yield percentages for the chemoselective product versus time. The optimized time catalyzed by each M-catalyst could be determined by circulating at the best reaction time in Figs. 6a-c. From Figs. 6a-c, the optimized time was 4 h (90%, with VOL) at 80°C. For ZrOL, it recorded 84% after 4 h and 86% after 4 h with ZnL at 90°C. Conclusively, the high reactivity of VOL with  $\text{V}^{4+}$  ions, high-valent oxy-metal ions, could be interpreted with high reversible electrochemical behavior, more valid oxidation states interchange and strong Lewis acid character. While,  $\text{Zr}^{4+}$ - and  $\text{Zn}^{2+}$ -catalysts have their high and stable valence and couldn't display extra-oxidation [25,45,47]. As well reported that the catalytic reactivity of the involved M-complex catalyst could be processed through electron and/or oxygen transfer mechanisms [48]. This could be taken place easily within VO-catalyst [45].

### 3.3.3. Solvent Effect

The catalytic potential of VO-, ZrO- and Zn-complex catalysts was influenced markedly by the nature of solvent in 1,2-cyclohexene epoxidation, as shown perviously [43]. The solvent effect was studied by acetonitrile, ethanol, chloroform, DMSO (dimethyl sulfoxide) or water in the epoxidation reactions under the optimized conditions for each M-catalyst, which presented in Table 2. The results in Table 2 showed that acetonitrile is the highest effective solvent in such a catalytic system (90 % catalyzed by VOL, 84% catalyzed by ZrOL and 85 % catalyzed by ZnL). Although acetonitrile is considered a labile coordinated ligand with various metal ions [48,49], it is a highly effective solvent for such epoxidation processes with aqueous  $\text{H}_2\text{O}_2$ , Table 2. Commonly, at high temperatures, acetonitrile is strongly stable in epoxidation processes compared to other applicable solvents without any observable reactivity towards any catalytic component, i.e. reactant and oxidant [44]. Acetonitrile with a high dielectric constant could progress the catalytic efficiency of  $\text{H}_2\text{O}_2$  within electron and oxygen transfer cycles [50]. In chloroform, the selectivity, conversion and yielding percentages of the targeted product were very good referring to the high catalytic reactivity of current M-catalysts at their optimized conditions. The yielding percentages of the chemoselective product with VOL, ZrOL and ZnL catalysts were 81, 72 and 77%, respectively. Due to strong organic nature and current M-complexes with less charge distribution in their molecules



**Scheme 2.** The aqueous hydrolysis of the epoxy product in  $\text{H}_2\text{O}$  in the catalytic system.

could be the reason for their less reactivity compared to that in acetonitrile. So, the less polarity of the reaction media in chloroform could reduce their catalytic progress within electron and/or oxygen transfer [51]. In ethanol, the conversion was close to 100%, but the selectivity was very good with VOL, ZrOL and ZnL catalyst (85, 60 and 77%, respectively). The reactivity of the catalytic systems was progressed in ethanol compared to that in chloroform. The recorded amount percentages of epoxy-1,2-cyclohexane were found 83, 57 and 70% using VOL, ZrOL and ZnL catalysts, respectively. Consequently, the catalytic reactions in chloroform and ethanol awarded close amounts of the chemoselective products with all M-catalysts.

In particular, dimethyl sulfoxide, DMSO, which is considered a high coordinated solvent, could bond to the central metal ion of the catalyst complex. This caused a high improvement in conversion percentages in catalyzed reactions within all M-catalysts (95–100%, Table 2). On the other hand, the selectivity and yielding percentages were low. Interestingly, the high coordination features of DMSO diminished also the catalytic efficiency of M-catalysts toward the oxidation selectivity [52] awarding 50, 58 and 67% of the epoxy product with VOL, ZrOL and ZnL, respectively. The high coordination ability of DMSO towards central metal ion in catalysts could bond and capsulate the catalyst and, hence, reduce the probability of a selective catalytic epoxidation [44].

In  $\text{H}_2\text{O}$ , the catalytic systems gave a moderate amount of the selective product (Table 2), 50, 41 and 44% with VOL, ZrOL and ZnL, respectively. The reactant is not soluble in water, hence, the reaction contents are not miscible enough in the epoxidation reaction to being activated. So, under an eco-friendly atmosphere (in water), the low polarity of M-catalyst and non-polar substrate (1,2-cyclohexene), may reduce notably their miscibility and then prohibit their catalytic reactivity [11,48]. Also, as well reported that the aqueous hydrolysis of the reactant and/or epoxy-product gave high amounts of undesired side products [53]. The aqueous hydrolysis of chemoselective products could improve the yield of the unwelcome side product (cyclohexane-1,2-diol), Scheme 2.

### 3.3.4. Oxidant Effect

With  $\text{H}_2\text{O}_2$ , *t*BuOOH or  $\text{NaClO}_4$ , as an oxygen source, the catalytic reactivity of the current VOL, ZrOL and ZnL catalysts toward epoxidation of 1,2-cyclohexene was examined and documented (Table 3). The obtained results illustrated that the 1,2-cyclohexene epoxidation processes could be controlled by the type of oxidant at optimized atmospheres in acetonitrile for each M-catalyst. From Table 3, *t*BuOOH afforded the best yield of epoxy-1,2-cyclohexane. *t*BuOOH is found to be the best oxidant for epoxidation under the applied catalysts that superior  $\text{H}_2\text{O}_2$ . The yields of epoxy-1,2-cyclohexane catalyzed by such catalysts with  $\text{H}_2\text{O}_2$  close to those with *t*BuOOH. Using *t*BuOOH, the catalytic processes afforded 94, 88 and 89% of epoxy-1,2-cyclohexane catalyzed by VOL, ZrOL and ZnL, respectively. With  $\text{H}_2\text{O}_2$ , the catalytic processes gave 90, 84 and 85% of chemoselective by VOL, ZrOL and ZnL, respectively. It is documented recently that *t*BuOOH is a more convenient oxidizing agent than the aqueous  $\text{H}_2\text{O}_2$  especially, in olefins epoxidation processes, due to its similar organic nature with the substrate in the reaction media [54]. To establish this behavior,  $\text{NaClO}_4$  oxidant with its high polarity was probed at the optimal atmosphere and

**Table 3**  
Oxidant type effect on the epoxidation of 1,2-cyclohexene by  $\text{H}_2\text{O}_2$ .

Catalyst <sup>a</sup>	Oxidant	Yield (%) <sup>b</sup>			Conversion (%)	Selectivity (%)
		R	P	Side products		
VOL	$\text{H}_2\text{O}_2$	0	90	10	100	90
	<i>t</i> BuOOH	0	94	6	100	94
	$\text{NaClO}_4$	10	53	37	90	59
ZrOL	$\text{H}_2\text{O}_2$	0	84	16	100	84
	<i>t</i> BuOOH	0	88	12	100	88
	$\text{NaClO}_4$	21	59	20	79	75
ZnL	$\text{H}_2\text{O}_2$	6	85	9	94	90
	<i>t</i> BuOOH	3	89	8	97	92
	$\text{NaClO}_4$	14	50	36	86	58

<sup>a</sup> The epoxidation of 1,2-cyclohexene (R) (1.0 mmol) by an aqueous  $\text{H}_2\text{O}_2$  (3.00 mmol), *t*BuOOH (1.7 mmol) or  $\text{NaClO}_4$  (1.7 mmol), catalyst (0.02 mmol) in 10 mL acetonitrile at the optimized reaction time and temperature.

<sup>b</sup> The percentages derived from GC results, selectivity control of P, epoxy-1,2-cyclohexane, and the other side products.

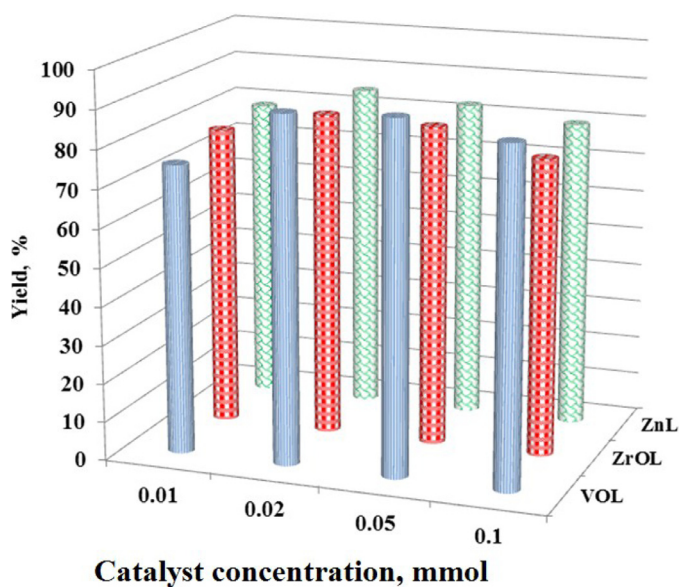


**Fig. 7.** The yield percentages of epoxy-1,2-cyclohexane of the epoxidation of 1,2-cyclohexene by an aqueous  $\text{H}_2\text{O}_2$  depending on the loaded amount (0.01, 0.02 mmol, 0.05 or 0.1 mmol) of the M-catalyst VOL, ZrOL or ZnL.

the results were listed in Table 3.  $\text{NaClO}_4$  gave less reactivity compared to those with *t*BuOOH or  $\text{H}_2\text{O}_2$ . The yields were found 53, 59 and 50% VOL, ZrOL and ZnL, respectively (Table 3).

It is noted that the processes with aqueous  $\text{H}_2\text{O}_2$  consumed relatively large stoichiometry, *i.e.* the excess amount of an aqueous  $\text{H}_2\text{O}_2$  compared to that of *t*BuOOH, because of a lot of water amounts inside (70% water). It could relatively reduce the potentiality of aqueous  $\text{H}_2\text{O}_2$  in comparison with *t*BuOOH [55]. The low potential of  $\text{NaClO}_4$  could reduce the catalytic reactivity of the VO-, ZrO- and Zn-catalysts due to less solubility in reaction media [54].

### 3.3.5. Effect of the M-catalyst amount

The catalytic activity of VOL, ZrOL and ZnL catalysts toward the current epoxidation reaction was examined as a function of the charged amount of M-catalysts, which listed (Table S7) and plotted (Fig. 7). The effect of VOL, ZrOL and ZnL amounts (0.01, 0.02, 0.05 and 0.1 mmol) was observed by the yield, conversion control and selectivity percentages (Fig. 7).

From Table S7, when the amount of catalyst was low, *i.e.* 0.01 mmol, the catalytic reactivity was moderate to good within 75, 78 and 79% using VOL, ZrOL and ZnL, respectively. The reaction system gave closed yield percentages when the loaded amount from

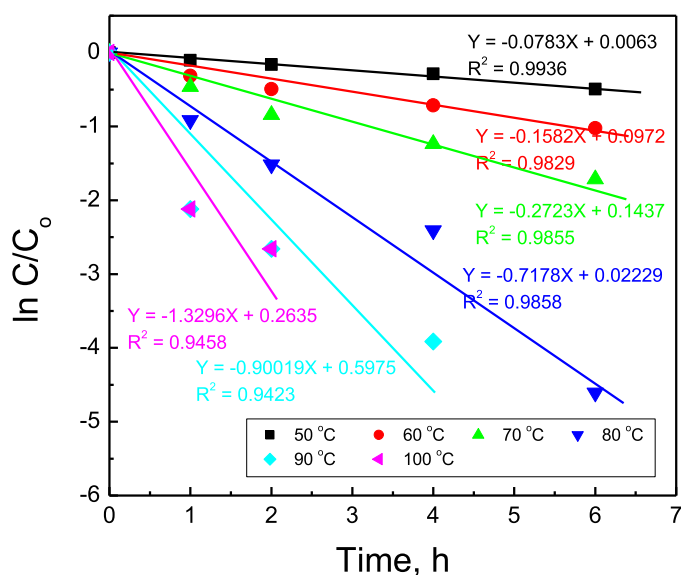


Fig. 8. The kinetic plots of the 1,2-cyclohexene epoxidation by  $\text{H}_2\text{O}_2$  catalyzed by ZnL as a function of temperature and time.

homogeneous catalysts was 0.02 and 0.05 mmol, as the optimized amount to produce the targeted product. The percentages of product were 90 and 91% (with 0.02 and 0.05 mmol of VOL), 84 and 83% (with 0.02 and 0.05 mmol of ZrOL) and 85 and 83% (with 0.02 and 0.05 mmol of ZnL), respectively. Conclusively, the best-loaded amount from homogeneous catalysts could be 0.02 and 0.05 mmol. However, the less loaded amount of catalysts, i.e. 0.01 mmol, was not enough to proceed. The overloaded amount of M-catalysts, i.e. 0.1 mmol, could strongly increase conversion but diminish the chemoselectivity percentages, as observed elsewhere [56].

### 3.3.6. Kinetics of epoxidation

The kinetic parameters of epoxidation for 1,2-cyclohexene at various temperatures (50, 60, 70, 80, 90 and 100°C) catalyzed by VO-, ZrO- or Zn-complex, as a pseudo-first-order reaction, were evaluated. The rate of catalytic reaction was evaluated from Eq. 5 and plotted in Fig. 8 (for ZnL) and Figs. S12a,b (for VOL and ZrOL, respectively).

$$-\ln\left(\frac{C}{C_0}\right) = kt \quad (5)$$

where, the initial concentration of 1,2-cyclohexene is  $C_0$ , the time is  $t$ , the catalytic rate constant is  $k$  and the residual concentration of 1,2-cyclohexene is  $C$ . The values of the rate constant were obtained from the slope in Figs. S13a,b,c. Additionally, within the Arrhenius equation, Eq. 6,  $E_a$ , the activation energy for catalytic epoxidation, was obtained by plotting  $\ln k$  against  $1/T$ ,  $T$  is the temperature in kelvin (Eq. 6).

$$\ln k = \ln A - \frac{E_a}{RT} \quad (6)$$

where, the gas constant is  $R$  and the pre-exponential factor is  $A$  [57]. The obtained magnitudes of  $E_a$  and  $A$  for epoxidation of 1,2-cyclooctene are listed in Table 4 for 50, 60, 70, 80, 90 and 100°C.

$$k = \frac{k_B T}{h} e^{-\Delta G^\# / RT} \quad (7)$$

where,  $h$  is Planck's constant and  $k_B$  is Boltzmann's constant. From Eq. 7, the average Gibb's free energy for epoxidation processes could be derived and then listed (Table 4). Hence, the  $E_a$  values assigned that VOL is the most effective catalyst compared to ZrOL and ZnL with the lowest  $E_a$  value (53.0  $\text{kJmol}^{-1}$ ). Also, the  $E_a$  value

Table 4

Kinetic parameters for 1,2-cyclohexene epoxidation by  $\text{H}_2\text{O}_2$  catalyzed M-complexes at optimized reaction conditions.

Complex	A x 10 <sup>8</sup>	$E_a$ , $\text{kJ mol}^{-1}$	$\Delta G^\#$
VOL	0.97	53.0	42.6
ZrOL	1.93	56.4	69.7
ZnL	2.36	57.2	70.1

of ZrOL catalyst (56.4  $\text{KJmol}^{-1}$ ) refers to higher catalytic potential of ZrOL compared to ZnL (57.2  $\text{KJmol}^{-1}$ ) with its high electrophilic character of  $\text{Zr}^{4+}$  ion in its complex catalyst over the low valent of  $\text{Zn}^{2+}$  ion in ZnL [12].

### 3.3.7. Epoxidation of other olefins

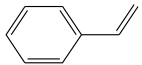
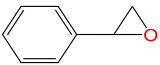
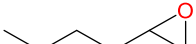
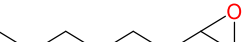
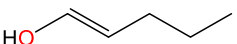
Screening of catalytic epoxidation for alternative olefins as cyclic and acyclic derivatives at the optimized atmosphere was examined and the obtained percentages of epoxy-target products are listed in Table 5. VO-, ZrO- and Zn-catalysts were used for such epoxidation reaction with aqueous  $\text{H}_2\text{O}_2$ . 1,2-Cyclohexene, 1,2-cyclooctene and styrene (as cyclic olefins with the strong electron-donating ability of the C=C group) presented high reactivity more than those of aliphatic or acyclic olefins (Table 5) [58]. The inner double-bonded C=C group could improve the reactivity of cyclic olefins compared to aliphatic olefins with terminal C=C double bond [58].

### 3.3.8. The proposed mechanism

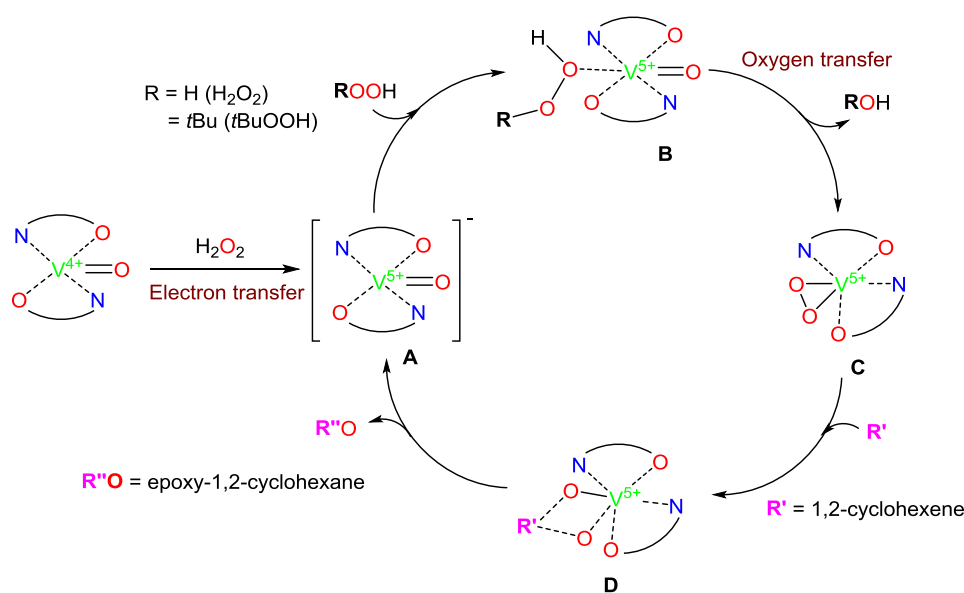
Geometrical characteristics of applied M-catalyst species with tetra-dentate coordinated  $\text{H}_2\text{L}$  ligand could help to understand the mechanistic pathway [25,55]. In the catalytic cycle, VOL with a square pyramidal geometry has an active vacant site capable of the coordination of oxidant molecule ( $\text{H}_2\text{O}_2$  or  $t\text{BuOOH}$ ). This could cause an electron transfer process within oxidation of  $\text{VO}^{2+}$  to highly reactive intermediate  $\text{VO}^{3+}$  species ( $\text{V}^{5+}$ , as strong electrophile) [23,59]. Another interaction of a new  $\text{H}_2\text{O}_2$  molecule with the electrophile **A** formed new active intermediate species (**B**) [60]. Then, within an oxygen transfer step from another  $\text{H}_2\text{O}_2$  to electrophile  $\text{V}^{5+}$  ion in **B** could give an active oxo- or peroxy-intermediate (**C**) with bridged O-O bonding, and liberating  $\text{H}_2\text{O}$  or  $t\text{BuOH}$  molecule [61]. The substrate molecule, **R'** (1,2-cyclohexene), could attract and bond to a strong electrophile  $\text{V}^{5+}$  ion in **C** to give a new intermediate (**D**) [11,12]. Formation of new intermediate species **D** caused oxidation for 1,2-cyclohexene to desired epoxy-1,2-cyclohexane (RO) with liberating and recycling of **A** (Scheme 3). The electron and oxygen transfer processes could be established practically by changing in characteristic VOL color in the reaction media when  $\text{H}_2\text{O}_2$  or  $t\text{BuOOH}$  was added. The observable repeated spectral changes of characteristic absorption spectra of VOL in acetonitrile (from 570 to 475 nm) were presented in Fig. 9, which was assigned for the formation of new intermediates.

The above mechanism could be not convenient for homogeneous catalytic systems for ZrOL and ZnL catalysts [47,62]. In particular, the electron transfer promotion could not be happened for ZrOL and ZnL due to the high stability of their valence as  $\text{Zr}^{4+}$  and  $\text{Zn}^{2+}$  ions (of  $d^0$  and  $d^{10}$  electronic configurations, respectively). This could be proven by UV-Vis spectral data. Spectral scans of ZrOL catalyst in reaction media, which did not show any significant changes in characteristic  $\lambda_{\text{max}}$  at 418 nm (Fig. 10). Consequently, another suggestion concerning ZrOL and ZnL catalytic mechanisms could be proposed [15]. The heterolytic or homolytic cleavage of oxidizing agent O-O bond could cause direct oxygen transfer to  $\text{M}^{2+}$ -catalyst awarding oxo-catalyst without an electron transfer process. The formed oxo-catalyst could transfer oxygen to the reactants to produce the target oxide-products, as shown in Scheme 4.

**Table 5**  
Epoxidation of some cyclic and acyclic alkenes catalyzed.

Entry	Alkene <sup>a</sup>	Product	Conversion, Selectivity %		
			VOL	ZrOL	ZnL
1			81 (85)	81 (76)	75 (80)
2			77 (79)	76 (75)	70 (73)
3			80 (79)	72 (71)	77 (79)
4			69 (55)	60 (51)	62 (53)
5			59 (47)	49 (39)	54 (44)
6			68 (42)	60 (41)	63 (39)

<sup>a</sup> Reaction carried out in acetonitrile (10 mL), alkene (1.0 mmol), H<sub>2</sub>O<sub>2</sub> (3.0 mmol) and catalyst (0.02 mmol) at the optimized condition for each catalyst.

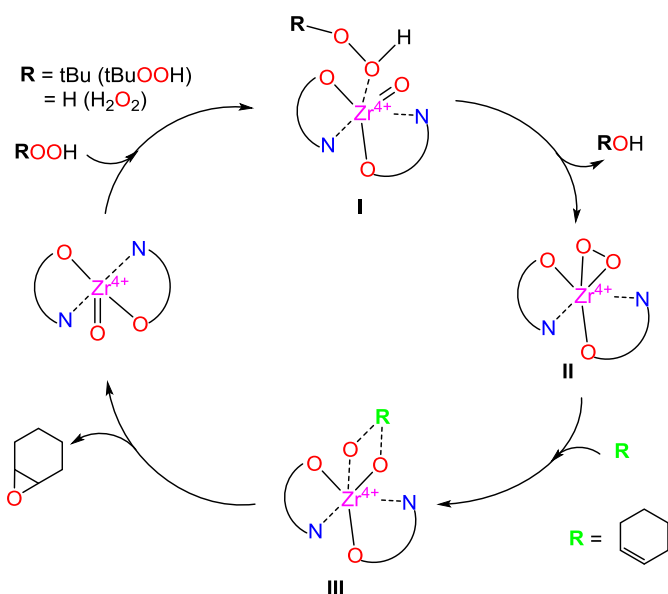
**Scheme 3.** The proposed mechanism for the epoxidation of 1,2-cyclohexene by aqueous H<sub>2</sub>O<sub>2</sub> under VO-catalysis, homogeneously.

The proposed mechanism described an attack of the oxidant molecule to central metal ion Zr<sup>4+</sup> or Zn<sup>2+</sup> and bonds then form intermediate I. The second step demonstrates the interaction of oxidant with intermediate I to form intermediate II, with liberating H<sub>2</sub>O or tBuOH molecule [18,21]. In which, bridged  $\mu$ -dioxygen of the intermediate could be formed within an oxygen transfer from oxidant to the central metal ion. Then, the substrate molecule brings close to each bridged  $\mu$ -dioxygen of the intermediate II by forming a new intermediate (III), which liberate the epoxy product (Scheme 4). The suggested mechanism is compatible with that of reported catalytic epoxidation of olefins by MoO<sub>2</sub>-complex catalysts [48,63].

From the mechanistic pathway, VOL catalyst exhibited the highest catalytic reactivity compared to those of other studied M-catalysts (ZrOL and ZnL). The electron transfer process improves significantly the reactivity of VOL with the highest chemoselectiv-

ity as less consumed time and less required temperature compared to those of ZrOL and ZnL catalysts (Tables S4-S6) [12,15,52].

The catalytic potential of the current M-complex catalysts (VOL, ZrOL and ZnL) could be estimated compared to other similar reported catalysts. VO(II)-dihydroindolone chelate showed respectable catalytic potential in the 1,2-cyclooctene epoxidation with aqueous H<sub>2</sub>O<sub>2</sub> yielding 87% of epoxy-1,2-cyclooctane after 3 h at 85°C [12]. Similar Zn<sup>2+</sup>- and VO<sup>2+</sup>-Schiff base complexes assigned high catalytic performance in the epoxidation of 1,2-cyclohexene awarding 82 and 92% of the selective product (in absence of Na<sup>+</sup>SO<sub>3</sub><sup>-</sup>-group) after 7 and 5 h at 85°C, respectively, and also 85 and 94% yields (in the presence of Na<sup>+</sup>SO<sub>3</sub><sup>-</sup>-group) after 6 and 4 h at 85°C, respectively [15]. VO-naphthalenylimino-phenolate complex catalyst displayed high reactivity for the 1,2-cyclohexene epoxidation with H<sub>2</sub>O<sub>2</sub>, which reported 93% yielding of the target product at 85°C after 1.5 h [38]. Hence, the current



**Scheme 4.** Catalytic cycle of the epoxidation of 1,2-cyclohexene catalyzed by ZrO- and Zn-catalysts.

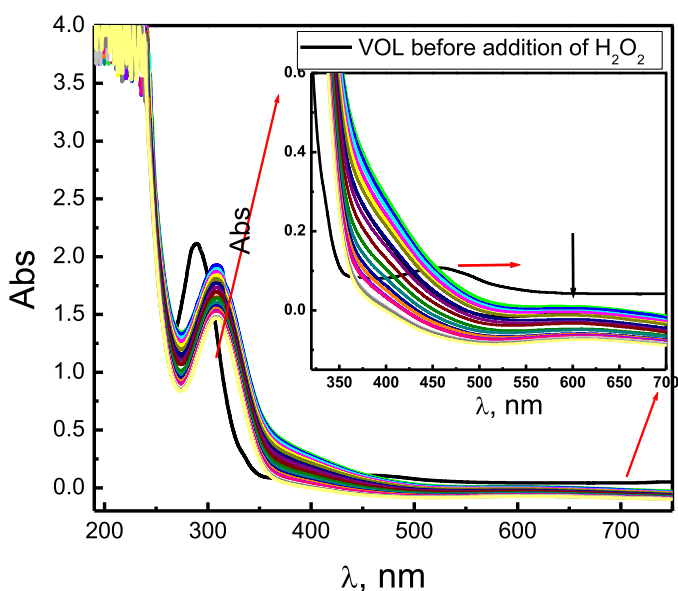


**Fig. 9.** Electronic spectral scans for VOL, as a catalyst for the epoxidation of 1,2-cyclohexene before and after addition of  $H_2O_2$  at the optimized conditions with interval time 10 min.

catalysts, specifically VOL, are considered active with convenient reaction conditions.

### 3.4. Oxidation of 2-aminothiophene

Oxidation of thiophenes is well documented with an alternative oxidizing agent under various atmospheres [48] to give two parallel main products, namely thiophene oxide and thiophene dioxide. Hence, the first attempt to identify all possible products for the oxidation of 2-aminothiophene (1.0 mmol), which carried out by using  $H_2O_2$  (3.0 mmol) and catalyzed by VOL, ZrOL or ZnL (0.02 mmol) under optimum conditions as 1,2-cyclohexene epoxidation. Types of detectable products and their yielding percentages were determined by GC/MS and shown in Table 6. Scheme 5 displays all possible products of 2-aminothiophene oxidation by  $H_2O_2$  and cat-

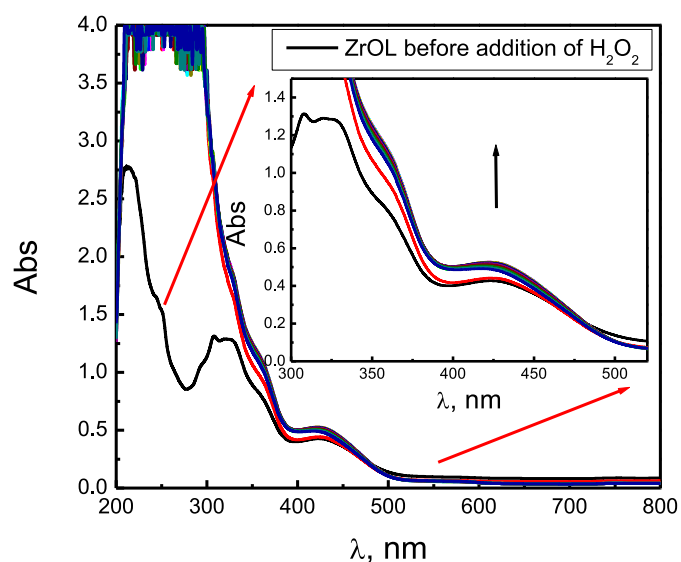
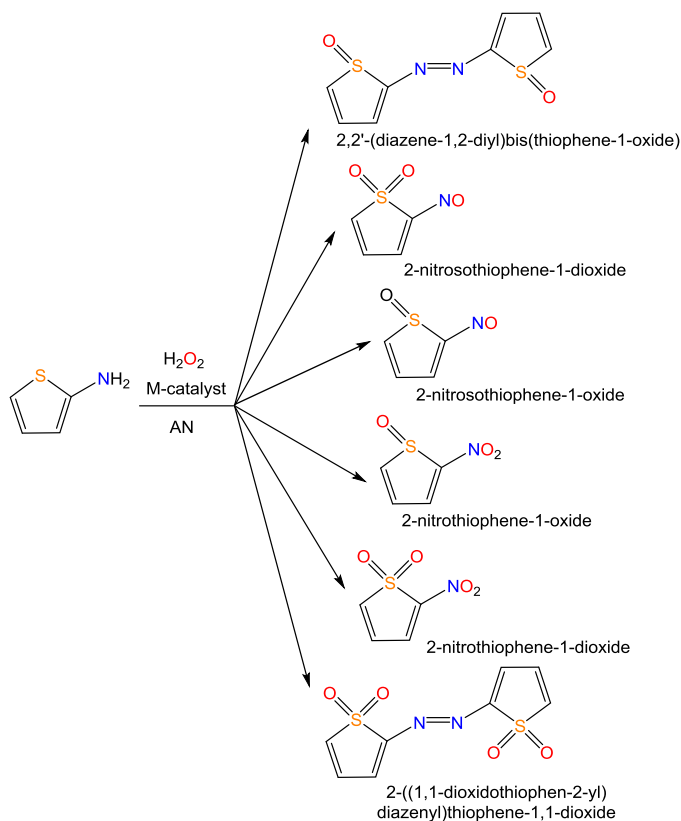


**Fig. 10.** Electronic spectral scans for ZrOL, as a catalyst for the epoxidation of 1,2-cyclohexene before and after addition of  $H_2O_2$  at the optimized conditions with interval time 10 min.



**Scheme 5.** All possible products of the oxidation of 2-aminothiophene using  $H_2O_2$  catalyzed by VOL, ZrOL or ZnL at their optimized reaction conditions.

alyzed by VOL, ZrOL or ZnL at their optimization. Additionally, the reaction in absence of a considered catalyst gave low conversion (15%) without a specific selective product.

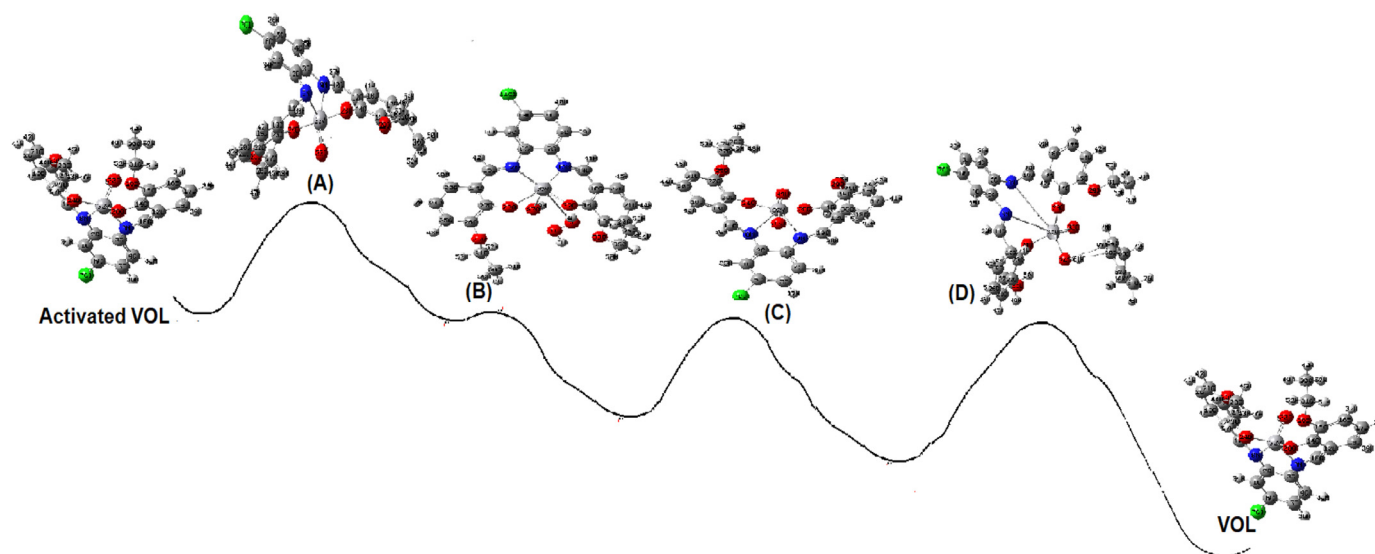
The catalytic oxidation of 2-aminothiophene was an unselective reaction, however, it gave some main products depending on the type of catalysts. With VOL, the highest yield percentages was the dioxy-dimeric form (2-((1,1-dioxidothiophen-2-yl)diazanyl)thiophene-1,1-dioxide) with 26%. On the other hand,

**Table 6**  
2-Aminothiophene oxidation catalyzed by VOL, ZrOL or ZnL using an aqueous H<sub>2</sub>O<sub>2</sub>.

Catalyst <sup>a</sup>	Conversion (%)	Reactant <sup>b</sup> 2-aminothiophene	2,2'-(diazene-1,2-diyl)bis(thiophene-1-oxide)	2-nitrosothiophene-1-dioxide	2-nitrosothiophene-1-oxide	2-nitrothiophene-1-oxide	2-nitrothiophene-1-dioxide	2-((1,1-dioxidothiophen-2-yl)diazenyl)thiophene-1,1-dioxide	Unknown side products
VOL	95	5	4	12	9	15	21	26	8
ZrOL	91	9	3	11	12	25	18	15	7
ZnL	88	12	--	8	10	21	20	19	10
No catalyst	19	81	--	4	--	--	4	5	7

<sup>a</sup> The oxidation of 2-aminothiophene (1.0 mmol) by an aqueous H<sub>2</sub>O<sub>2</sub> (3.00 mmol), catalyst (0.02 mmol) in 10 mL solvent at the optimized reaction time and temperature for each M-catalyst.

<sup>b</sup> The percentages derived from GC/MS results.

**Scheme 6.** Profile for activated intermediates corresponds to the epoxidation of 1,2-cyclohexene by aqueous H<sub>2</sub>O<sub>2</sub> under VO-catalysis, homogeneously.

the main product of oxidation reaction with ZrOL and ZnL was 2-nitrothiophene-1-oxide. The central metal ion in its catalyst complex played a prominent role in the selectivity of the oxidation product.

### 3.5. Supporting computations

#### 3.5.1. Quantitative Structural Activity relationships (QSAR)

QSAR indexes were achieved for the current complexes using HyperChem (8.1) software through successive steps required for energy minimization. Such steps were, adding H-atoms, setup of semi-empirical (AM1), setup force-field Molecular Mechanics (MM<sup>+</sup>) and then minimization was proceeded. This study was accomplished without fixing any parameter and finished over the Polake-Ribiere conjugated gradient algorithm method [64]. The reactivity, polarizability, surface area, hydration energy and partition coefficient (log p), were calculated for the investigated complexes and reported in Table 7. The factors that reflect surface characteristics of the M-complexes are what give an impression of the expected catalytic behavior. Such factors are the reactivity, polarizability and surface area. The superiority of the ZnL complex was recorded, while VOL and ZrOL appeared with similar and moderate characteristics. Although this superiority may not be useful in the current catalytic epoxidation systems, due to the lack of zinc's ability to oxidize and enter into a catalytic cycle that requires its oxidation as a first stage.

**Table 7**  
QSAR parameters for VO, ZrO and Zn-complexes.

The parameters	Complexes		
	VOL	ZnL	ZrOL
Surface area (grid) (Å)	633.40	642.82	625.78
Volume(Å)	1204.04	1213.40	1185.66
Hydration energy (k cal/mol)	-12.65	-12.88	-13.83
Log p	-1.88	-3.67	1.88
Reactivity (Å)	129.47	131.19	129.47
Polarizability (Å)	46.05	46.95	46.04

#### 3.5.2. Global reactivity of optimized geometries

DFT was applied using Becke3-Lee-Yang-Parr (B3LYP) exchange-correlation functional under 6-311G<sup>++</sup> basis set due to the accuracy, flexibility and consistency. Better performance was progressed by valence double-zeta polarized basis set (6-311G<sup>++</sup>), which adds to 6-31G set five functions known as d-type Cartesian-Gaussian polarization, on each atom. This computation aims to demonstrate the best structural forms for VOL, ZrOL and ZnL complexes and calculate important parameters. Many characteristics could appear that favor the best for the catalytic application, as well as, obtaining electrostatic maps to know the extent of the susceptibility to acquiring electrons from the external environment. All extracted files were visualized to obtain

such requirements and studied to distinguish the main differences between the M-complexes. The optimized structures (Fig. S8) showed natural bonds without strain and two central metals (VO & ZrO) appeared not crowded, which may allow them to add an extra bond. Also, electrophilicity ( $\omega$ ), absolute-softness ( $\sigma$ ), global softness ( $S$ ) and electronegativity ( $\chi$ ) indexes were calculated to set an expectation for closest characteristics for complexes (Table S3) [65]. High electronegativity and global softness coupled with low electrophilicity of VOL complex, reflect its inability to acquire electrons from surrounding acquiring but has high ability for binding with any donor atom, the small size of vanadium is a supporter. Dipole moment ( $D_{\text{debye}}$ ), formation energy ( $E$ , a.u.) and oscillator strength ( $f$ ) were taken from log files. Low dipole moment and formation energy reflect low polarity over the complex surface and high stability recorded with VOL, respectively. Also, the high oscillator strength value of VOL complex reflects the labile nature of the  $d^1$  electron, which relocated from its orbital easily (Fig. S9).

**3.5.2.1. Electrostatic potential features.** Using fchk file and upon new cubic contours, HOMO & LUMO, MEP and iso-surface maps were created, to distinguish electron density distribution on the whole complexes. HOMO and LUMO levels (Fig. 4) were appeared extending over the entire complexes and the highly concentrated around the environment of the central atom. This verifies the impact of metal ions on electronic transitions inside the complex [66]. The charges on atoms of each M-complex were calculated and graphed (Fig. S10), to identify the changes on coordinating atoms (N8, N9, O24, O28 & M) after bonding. Regarding VOL, the charges on N8, N9, O24 & O28 were enhanced due to M-LCT, while in other complexes, such atoms suffer minimization in their negativity, due to L-MCT. This indicates the flexibility of the vanadium electron cloud, which exerted from the labile electron at the Fermi level.

Molecular electrostatic potential maps (MEP) were created (Fig. 5) to evaluate electron density features over functional groups. Electrophilic (electron-poor), nucleophilic or neutral potential zones were clearly differentiated chromatically by blue, red and green colors, respectively. Nucleophilicity as the electron-rich zone was remarked around VO, while ZrOL and ZnL complexes such feature has slightly appeared with prevailing neutrality one [67]. This indicates that the vanadium surrounding is electron-rich and could easily lose electrons. Furthermore, iso-surface maps were created with the presence of electron distribution array plots (Fig. S11). This map type was obtained by determining electron density over multi-points on the surface grid and then connected to build the electrostatic contour. Yellow lines in the array plot point to the electron-rich area (inner contour) and the red lines point to the electrons-poor area (outer contour). The surface boundary of VOL displayed broad red lines, which denotes its unsaturated surface compared to that of the others [68].

### 3.5.3. DFT studies support catalytic feature

Commonly, the catalytic process oxidation-based systems are controlled by different features that belong to the electronic configuration and its distribution over the applied catalyst. So, the computation studies achieve importance in supporting of the suggested mechanism, which based mainly on the logical assumption of how the catalytic process will happen. All suggested intermediates faced geometry optimization under 6-31G++ basis set, to put a suitable view for catalytic behavior. VOL catalyst ( $E = -2815.806$  a.u.,  $D = 3.37$  Debye), which activated initially under optimal conditions, raises the energy level of the stabilized catalyst. An intermediate A ( $E = -2817.111$  a.u.,  $D = 7.51$  Debye) appeared with the closest stability with initial VO(II) form, but has a high polarity that facilitates its coordination with  $H_2O_2$ . Conformer B

( $E = -2968.394$  a.u.,  $D = 15.066$  Debye) displayed with high stability, which pushed to proceed in the catalytic cycle, further its polarity is remarkably increased. Conformer C ( $E = -2892.177$  a.u.,  $D = 8.806$  Debye) appeared with reduced stability and polarity, which denotes its faster conversion. Conformer D ( $E = -2881.177$  a.u.,  $D = 8.776$  Debye) appeared close in the stability and polarity of conformer C, which also has the same ability for faster conversion to intermediate A, conducting to the original free catalyst. The success of VOL complex in oxidation-based catalytic reactions mainly depends on different factors as follows; i) Ease of  $V^{4+}$  ion oxidation. ii) Free z-axis for extra-bonds and removal of crystal water molecules, which happened under the optimal conditions (up to  $80^\circ\text{C}$ ). This may evacuate sites inside the molecular building and then adsorb  $H_2O_2$  molecule, as an introductory step before bonding.

## 4. Conclusions

In this work, ZrO(II), VO(II) and Zn(II) complexes have been successfully synthesized from an asymmetrical tetra-dentate ligand. These compounds were characterized by all available tools (analytical, spectral and theoretical). Distorted octahedral geometry was proposed for Zn(II) complex, while square pyramidal geometries were proposed for ZrO(II) and VO(II) complexes. In a catalytic application using M-complexes under  $H_2O_2$ , as an oxidant, for the epoxidation of 1,2-cyclohexene, we found that our three complexes exhibited moderate to very good catalytic control. Parameters such as temperature, time, solvent, oxidant and amount of M-catalysts were changed to show different catalytic effects on both activity and selectivity of the oxidative process. The catalysts screening for the epoxidation of various alkenes within cyclic and acyclic chains at optimization was studied. All M-catalysts were efficiently capable of catalyzing epoxidation of those alkenes to their corresponding epoxy products by aqueous  $H_2O_2$ . But the superiority of VO(II) complex in the catalytic role in studied epoxidation reactions, was clearly noticed. Also, the first attempt for catalytic oxidation of 2-aminothiophene using  $H_2O_2$  and catalyzed by VOL, ZrOL and ZnL, was reported. Various products with high conversion and less selectivity were obtained and defined by GC/MS. Moreover, it is worthy to note that the computational implementations as QSAR and DFT study, mostly throw a shadow on distinguishing characteristics of VO(II) complex in comparison with the others. The catalytic pathways proposed were confirmed by DFT studies.

### Declaration of Competing Interest

No.

### CRediT authorship contribution statement

**Mohamed Shaker S. Adam:** Conceptualization, Methodology, Formal analysis, Investigation, Writing - original draft, Writing - review & editing, Supervision. **Laila H. Abdel-Rahman:** Software, Data curation, Writing - original draft. **Hanan El-Sayed Ahmed:** Methodology, Data curation, Validation, Resources, Writing - review & editing. **M.M. Makhoulouf:** Conceptualization, Formal analysis, Project administration, Funding acquisition, Software, Data curation, Visualization. **Mona Alhasani:** Software, Writing - original draft. **Nashwa M. El-Metwaly:** Methodology, Validation, Resources, Writing - original draft, Writing - review & editing, Supervision.

### Acknowledgment

Taif University Researchers Supporting Project number (TURSP-2020/165), Taif University, Taif, Saudi Arabia.

## Supplementary materials

Supplementary material associated with this article can be found, in the online version, at doi:10.1016/j.molstruc.2021.130295.

## References

- [1] K.C. Gupta, A.K. Sutar, Catalytic activities of Schiff base transition metal complexes, *Coord. Chem. Rev.* 252 (2008) 1420–1450.
- [2] (a) M. Hajrezaie, M. Paydar, C.Y. Looi, S.Z. Moghadamtousi, P. Hassandarvish, M.S. Salga, H. Karimian, K. Shams, M. Zahedifard, N.A. Majid, H.M. Ali, M.A. Abdulla, Apoptotic effect of novel Schiff Based  $\text{CdCl}_2(\text{C}_{14}\text{H}_{21}\text{N}_3\text{O}_2)$  complex is mediated via activation of the mitochondrial pathway in colon cancer cells, *Sci. Rep.* 5 (2015) 9097; (b) M.S.S. Adam, H. Elsayy, Biological potential of oxovanadium salicylideneamino-acid complexes as cytotoxic, antimicrobial, antioxidant and DNA interaction, *J. Photochem. Photobiol. B* 184 (2018) 34–43.
- [3] (a) D. Gong, B. Wang, X. Jia, X. Zhang, The enhanced catalytic performance of cobalt catalysts towards butadiene polymerization by introducing a labile donor in a salen ligand, *Dalton Trans* 43 (2014) 4169–4178; (b) M.S.S. Adam, O.M. El-Hady, F. Ullah, Biological and catalytic potential of sustainable low and high valent metal-Schiff base sulfonate salicylidene pincer complexes, *RSC Adv* 9 (2019) 34311–34329.
- [4] L. Zhou, C.C. Kwok, G. Cheng, H. Zhang, C.M. Che, Efficient red organic electro-luminescent devices by doping platinum(II) Schiff base emitter into two host materials with stepwise energy levels, *Opt. Lett.* 38 (2013) 2373–2375.
- [5] (a) S.A. Lee, G.R. You, Y.W. Choi, H.Y. Jo, A.R. Kim, I. Noh, S.J. Kim, Y. Kim, C. Kim, A new multifunctional Schiff base as a fluorescence sensor for  $\text{Al}^{3+}$  and a colorimetric sensor for  $\text{CN}^-$  in aqueous media: an application to bioimaging, *Dalton Trans* 43 (2014) 6650–6659; (b) A. Ganguly, B.K. Paul, S. Ghosh, S. Kar, N. Guchhait, Selective fluorescence sensing of Cu(II) and Zn(II) using a new Schiff base-derived model compound: naked eye detection and spectral deciphering of the mechanism of sensory action, *Analyst* 138 (2013) 6532–6541.
- [6] (a) C.R. Nayar, R. Ravikumar, Review: Second order nonlinearities of Schiff bases derived from salicylaldehyde and their metal complexes, *J. Coord. Chem.* 67 (2014) 1–16; (b) M.M. Makhlof, H. Alburaihi, M.M. Shehata, M.S.S. Adam, M.M. Mostafa, A. El-Denglawy, Synthesis, physicochemical and optical characterization of a new isatin hydrazone derivative and its ZnO-complex for potential energy conversion and storage applications, *J. Phys. Chem. Solids* 151 (2021) 109817.
- [7] W. Al Zoubi, N. Al Mohanna, Membrane sensors based on Schiff bases as chelating ionophores – A review, *Spectrochim. Acta A* 132 (2014) 854–870.
- [8] (a) A.W. Jeevadason, K.K. Murugavel, M.A. Neelakantan, Review on Schiff bases and their metal complexes as organic photovoltaic materials, *Renew. Sustain. Energy Rev.* 36 (2014) 220–227; (b) M.M. Shehata, M.S.S. Adam, K. Abdelhady, M.M. Makhlof, Facile synthesis, characterizations, and impedance spectroscopic features of Zn(II)-bis Schiff base complex films towards, *J. Solid Stat. Electrochem.* 23 (2019) 2519–2531.
- [9] R.M. Clarke, T. Storr, The chemistry and applications of multimetallic salen complexes, *Dalton Trans* 43 (2014) 9380–9391.
- [10] (a) X. Liu, C. Manzur, N. Novoa, S. Celedón, D. Carrillo, J.-R. Hamon, Multidentate unsymmetrically-substituted Schiff bases and their metal complexes: Synthesis, functional materials properties, and applications to catalysis, *Coord. Chem. Rev.* 357 (2018) 144–172; (b) S. Bertini, A. Coletti, B. Floris, V. Conte, P. Galloni, Investigation of VO-salophen complexes electronic structure, *J. Inorg. Biochem.* 147 (2015) 44–53.
- [11] M.F.I. Al-Hussein, M.S.S. Adam, Catalytic evaluation of copper (II) N-salicylidene-amino acid Schiff base in the various catalytic processes, *Appl. Organomet. Chem.* 34 (2020) e5598.
- [12] M.S.S. Adam, Catalytic activity of nickel(II), copper(II) and oxovanadium(II)-dihydroindolone complexes towards homogeneous oxidation reactions, *Appl. Organomet. Chem.* 32 (2018) e4234.
- [13] M. Mandal, V. Nagaraju, G.V. Karunakar, B. Sarma, B.J. Borah, K.K. Bania, Electronic, Conjugation, and Confinement Effects on Structure, Redox, and Catalytic Behavior of Oxido-Vanadium(IV) and (-V) Chiral Schiff Base Complexes, *J. Phys. Chem. C* 119 (2015) 28854–28870.
- [14] (a) G. Licini, V. Conte, A. Coletti, M. Mba, C. Zonta, Recent advances in vanadium catalyzed oxygen transfer reactions, *Coord. Chem. Rev.* 255 (2011) 2345–2357; (b) M. Sutradhar, L.M.D.R.S. Martins, M.F.C.G.da Silva, A.J.L. Pombeiro, Vanadium complexes: Recent progress in oxidation catalysis, *Coord. Chem. Rev.* 301–302 (2015) 200–239.
- [15] M.S.S. Adam, M.A. Al-Omair, F. Ullah, Catalytic comparison of various polar Zn(II)- and VO(II)-Schiff base complexes in (ep)oxidation processes of 1,2-cyclohexene and cyclohexane, *Res. Chem. Intermediat.* 45 (2019) 4653–4675.
- [16] C.I. Fernandes, P.D. Vaz, T.G. Nunes, C.D. Nunes, Zinc biomimetic catalysts for epoxidation of olefins with  $\text{H}_2\text{O}_2$ , *Appl. Clay Sci.* 190 (2020) 105562.
- [17] (a) J. Huang, J. Xie, J. Cai, Asymmetric epoxidation of unfunctionalized olefins catalyzed by chiral salen-Mn(III) immobilized on alkoxy-modified ZnPS-PVPA, *Appl. Organomet. Chem.* 33 (2019) e4982; (b) J. Huang, X. Fu, Q. Miao, Catalytic asymmetric epoxidation of unfunctionalized olefins using a series novel type of layered crystalline organic polymer-inorganic hybrid zinc phosphate-phosphate immobilized aryldiamine modified chiral salen Mn(III) complex, *Appl. Catal. A* 407 (2011) 163–172.
- [18] (a) M. Liu, S. Qiu, Y. Ye, G. Yin, Mild and efficient synthesis of isoindigo derivatives catalyzed by Lewis acid, *Tetrahedron Lett* 57 (2016) 5856–5858; (b) M. Khorshidifard, H.A. Rudbari, B. Askari, M. Sahihi, M.R. Farsani, F. Jalilian, G. Bruno, Cobalt(II), copper(II), zinc(II) and palladium(II) Schiff base complexes: Synthesis, characterization and catalytic performance in selective oxidation of sulfides using hydrogen peroxide under solvent-free conditions, *Polyhedron* 95 (2015) 1–13.
- [19] A.T. Normand, R. Malacea-Kabbara, R. Lapenta, A. Dajnak, P. Richard, H. Catey, A. Bolley, A. Grassi, S. Milione, A. Auffrant, S. Dagorne, P. Le Gendre, Phosphalene group IV metal complexes: synthesis, characterization and ring opening polymerization of lactide, *Dalton Trans* 49 (2020) 6989–7004.
- [20] C.-J. Yu, C.-Y. Li, C.-Y. Tsai, B.-T. Ko, Titanium, zirconium and hafnium complexes bearing amino-benzotriazole phenolate ligands as efficient catalysts for ring-opening polymerization of lactides, *Inorg. Chem. Commun.* 109 (2019) 107561.
- [21] M. Mandal, V. Ramkumar, D. Chakraborty, Salen complexes of zirconium and hafnium: synthesis, structural characterization and polymerization studies, *Polym. Chem.* 10 (2019) 3444–3460.
- [22] M. Sedighipoor, A.H. Kianfar, W.A.K. Mahmood, M.H. Azarian, Epoxidation of alkenes by an oxidovanadium(IV) tetradentate Schiff base complex as an efficient catalyst with *tert*-butyl hydroperoxide, *Inorg. Chim. Acta* 457 (2017) 116–121.
- [23] M. Aschi, M. Crucianelli, A.D. Giuseppe, C.D. Nicola, F. Marchetti, Insights on the mechanistic features of catalytic oxidations of simple and conjugated olefins promoted by  $\text{VO}(\text{acac})_2/\text{H}_2\text{O}_2$  system, in acetonitrile: A computational study, *Catal. Today* 192 (2012) 56–62.
- [24] N. Xing, L.T. Xu, F.Y. Bai, H. Shan, Y.H. Xing, Z. Shi, Synthesis and characterization of novel transition metal complexes with indole acetic acid ligands: Evaluation of their catalytic activity for the oxidation of cyclohexane, *Inorg. Chim. Acta* 409 (2014) 360–366.
- [25] W. Wang, D. Agustin, R. Poli, Influence of ligand substitution on molybdenum catalysts with tridentate Schiff base ligands for the organic solvent-free oxidation of limonene using aqueous TBHP as oxidant, *Mol. Catal.* 443 (2017) 52–59.
- [26] H. Hartmann, P. Gerstner, D. Rohde, A Simple Route to N-Arylated 2-Amino-1-phenolates as a New Class of Amorphous Glass Forming Molecules, *Org. Lett.* 3 (2001) 1673–1675.
- [27] (a) R.F.M. Elshaarawy, I.M. Eldeen, E.M. Hassan, Efficient synthesis and evaluation of bis-pyridinium/bis-quinolinium metallosalophens as antibiotic and antitumor candidates, *J. Mol. Struct.* 1128 (2017) 162–173; (b) R. Hernandez-Molina, A. Mederos, S. Dominguez, P. Gili, C. Ruiz-Perez, A. Castineiras, X. Solans, F. Lloret, J.A. Real, Different Ground Spin States in Iron(III) Complexes with Quadridentate Schiff Bases: Synthesis, Crystal Structures, and Magnetic Properties, *Inorg. Chem.* 37 (1998) 5102–5108; (c) K. Sampath, C. Jayabalakrishnan, Ruthenium(II) Tetradentate Schiff Base Complexes: Synthesis, Characterization, DNA Binding, and Antioxidant Studies, *Synth. React. Inorg. Met.-Org. Nano-Met. Chem.* 45 (2015) 1145–1153.
- [28] V.R. Chandrasekhar, K.M. Palsamy, R. Lokesh, D.T. Thangadurai, G.N. Indra, R. Jegathalaprathaban, R. Gurusamy, Biomolecular docking, antimicrobial and cytotoxic studies on new bidentate schiff base ligand derived metal (II) complexes, *Appl. Organomet. Chem.* 33 (2019) e4753.
- [29] A.S. Munde, A.N. Jagdale, S.M. Jadhav, T.K. Chondhekar, Synthesis, characterization and thermal study of some transition metal complexes of an asymmetrical tetradentate Schiff base ligand, *J. Serb. Chem. Soc.* 75 (2010) 349–359.
- [30] M. J. Frisch, G. W. Trucks, H. B. Schlegel, G. E. Scuseria, M. A. Robb, J. R. Cheeseman, G. Scalmani, V. Barone, B. Mennucci, G. A. Petersson, H. Nakatsuji, M. Caricato, X. Li, H. P. Hratchian, A. F. Izmaylov, J. Bloino, G. Zheng, J. L. Sonnenberg, M. Hada, M. Ehara, K. Toyota, R. Fukuda, J. Hasegawa, M. Ishida, T. Nakajima, Y. Honda, O. Kitao, H. Nakai, T. Vreven, J. A. Montgomery, J. E. Peralta, F. Ogliaro, M. Bearpark, J. J. Heyd, E. Brothers, K. N. Kudin, V. N. Staroverov, T. Keith, R. Kobayashi, J. Normand, K. Raghavachari, A. Rendell, J. C. Burant, S. S. Iyengar, J. Tomasi, M. Cossi, N. Rega, J. M. Millam, M. Klene, J. E. Knox, J. B. Cross, V. Bakken, C. Adamo, J. Jaramillo, R. Gomperts, R. E. Stratmann, O. Yazyev, A. J. Austin, R. Cammi, C. Pomelli, J. W. Ochterski, R. L. Martin, K. Morokuma, V. G. Zakrzewski, G. A. Voth, P. Salvador, J. J. Dannenberg, S. Dapprich, A. D. Daniels, O. Farkas, J. B. Foresman, J. V. Ortiz, J. Cioslowski, D. J. Fox, Gaussian, Inc., Wallingford CT (2010).
- [31] (a) B.G. Johnson, M.J. Frisch, Analytic second derivatives of the gradient-corrected density functional energy. Effect of quadrature weight derivatives, *Chem. Phys. Lett.* 216 (1993) 133–140; (b) F. Weigend, R. Ahlrichs, Balanced basis sets of split valence, triple zeta valence and quadruple zeta valence quality for H to Rn: Design and assessment of accuracy, *Phys. Chem. Chem. Phys.* 7 (2005) 3297–3305.
- [32] S.A. Khan, K. Rizwan, S. Shahid, M.A. Noamaan, T. Rasheed, H. Amjad, Synthesis, DFT, computational exploration of chemical reactivity, molecular docking studies of novel formazan metal complexes and their biological applications, *Appl. Organomet. Chem.* 34 (2020) e5444.
- [33] R. Dennington II, T. Keith, J. Millam, GaussView, Semichem Inc., Shawnee Mission, KS, 2007 Version 4.1.2.
- [34] R.C. Chikate, S.B. Padhye, Transition metal quinone-thiosemicarbazone complexes 2: Magnetism, ESR and redox behavior of iron (II), iron (III), cobalt (II) and copper (II) complexes of 2-thiosemicarbazido-1,4-naphthoquinone, *Polyhedron* 24 (2005) 1689–1700.
- [35] (a) B. Geeta, K. Shrivankumar, P.M. Reddy, E. Ravikrishna, M. Saranganani, K.K. Reddy, V. Ravindera, Binuclear cobalt(II), nickel(II), copper(II) and palladium(II) complexes of a new Schiff-base as ligand: Synthesis, structural characterization, and antibacterial activity, *Spectrochim. Acta A* 77 (2010) 911–915; (b) M.S.S. Adam, L.H. Abdel-Rahman, A.M. Abu-Dief, N.A. Hashem, Synthesis,

- catalysis, antimicrobial activity and DNA interactions of new Cu(II)-Schiff base complexes, *Inorg. Nano-Met. Chem.* 50 (2020) 136–150.
- [36] (a) M.S.S. Adam, M.M. Youssef, M.F. Abo Elghar, A.M. Hafez, U. El-Ayaan, Synthesis and characterization of binary and ternary oxovanadium complexes of N,N'-(2-pyridyl)thiourea and curcumin. Catalytic oxidation potential, antibacterial, antimicrobial, antioxidant and DNA interaction studies, *Appl. Organometal. Chem.* 31 (2017) e3650; (b) M.S.S. Adam, Sustainable bipolar homo-dicopper (II) dihydrazone complex as a catalyst for Sonogashira cross couplings, *J. Organomet. Chem.* 903 (2019) 120985.
- [37] W.A. Zordok, Synthesis, spectroscopic, structural characterization, thermal analysis, kinetics, biological evaluation of non-steroidal anti-inflammatory drug diclofenac zirconium (IV) solvates (L) (L ¼ H<sub>2</sub>O, DMF, Py and Et<sub>3</sub>N), *J. Mol. Struct.* 1166 (2018) 270–285.
- [38] M.S.S. Adam, M.M. Makhlof, F. Ullah, A.D.M. Mohamad, Catalytic and biological reactivities of mononuclear copper (II) and vanadyl (II) complexes of naphthalenylimino-phenolate sodium sulfonate, *J. Taiwan Inst. Chem. Eng.* 118 (2021) 12–28.
- [39] M.S.S. Adam, A.D.M. Mohamad, Catalytic (ep)oxidation and corrosion inhibition potentials of Cu<sup>II</sup> and Co<sup>II</sup> pyridinylimino phenolate complexes, *Polyhedron* 151 (2018) 118–130.
- [40] L.H. Abdel-Rahman, M.S.S. Adam, A.M. Abu-Dief, H. Moustafa, M.T. Basha, A.S. Aboraia, B.S. Al-Farhan, H.E. Ahmed, Synthesis, theoretical investigations, biocidal screening, DNA binding, in vitro cytotoxicity and molecular docking of novel Cu(II), Pd(II) and Ag(I) chlorobenzylidene Schiff base: Promising antibiotic and anticancer agents, *Appl. Organometal. Chem.* 32 (2018) e4527.
- [41] (a) M. Gaber, Y. El-Sayed, K. El-Baradie, R. Fahmy, Cu(II) complexes of monobasic bi- or tridentate (NO, NNO) azo dye ligands: synthesis, characterization, and interaction with Cu-nanoparticles, *J. Mol. Struct.* 1032 (2013) 185–194; (b) M. Montazerzohori, S. Mojahedjahreni, A. Masoudiasl, P. McArdle, Nano structure zinc (II) Schiff base complexes of a N3-tridentate ligand as new biological active agents: Spectral, thermal behaviors and crystal structure of zinc azide complex, *Spectrochim. Acta A* 5 (2015) 517–528.
- [42] H. Katouah, A.M. Hameed, A. Alharbi, F. Alkhatib, R. Shah, S. Alzahrani, R. Zaky, N.M. El-Metwaly, Green Synthesis Strategy for New Schiff-Base Complexes: Characterization, Conductometry, In Vitro Assay Confirmed by In Silico Approach, *ChemistrySelect* 5 (2020) 10256–10268.
- [43] (a) M. Kiriara, Aerobic oxidation of organic compounds catalyzed by vanadium compounds, *Coord. Chem. Rev.* 255 (2011) 2281–2302; (b) J.A.L. da Silva, J.J.R.F. da Silva, A.J.L. Pombeiro, Oxovanadium complexes in catalytic oxidations, *Coord. Chem. Rev.* 255 (2011) 2232–2248.
- [44] M.S.S. Adam, A.M. Hafez, I. El-Ghamry, Catalytic performance of binary and ternary oxovanadium complexes of dipyrindinyl-urea in (ep)oxidation of cis-cyclooctene and 1-octene, *Reac. Kinet. Mech. Cat.* 124 (2018) 779–805.
- [45] N. Mizuno, K. Kamata, Catalytic oxidation of hydrocarbons with hydrogen peroxide by vanadium-based polyoxometalates, *Coord. Chem. Rev.* 255 (2011) 2358–2370.
- [46] L.S. Yuan, R. Razali, J. Efendi, N.A. Buang, H. Nur, Temperature-controlled selectivity in oxidation of 1-octene by using aqueous hydrogen peroxide in phase-boundary catalytic system, *Appl. Catal. A* 460–461 (2013) 21–25.
- [47] H. Han, L. Lu, Q. Wang, M. Zhu, C. Yuan, S. Xing, X. Fu, Synthesis and evaluation of oxovanadium(IV) complexes of Schiff-base condensates from 5-substituted-2-hydroxybenzaldehyde and 2-substituted-benzenamine as, selective inhibitors of protein tyrosine phosphatase 1B, *Dalton Trans* 41 (2012) 11116–11124.
- [48] M.S.S. Adam, M.S.M. Ahmed, O.M. El-Hady, S. Shaaban, Bis-dioxomolybdenum (VI) oxalyldihydrazone complexes: Synthesis, characterization, DFT studies, catalytic epoxidation potential, molecular modeling and biological evaluations *Appl. Organomet. Chem.* 34 (2020) e5573.
- [49] (a) G. Grivani, V. Tahmasebi, A.D. Khalaji, K. Fejfarova, M. Dušek, Synthesis, characterization and crystal structure determination of a new vanadium(IV) Schiff base complex (VOL2) and investigation of its catalytic activity in the epoxidation of cyclooctene, *Polyhedron* 51 (2013) 54–60; (b) G. Grivani, A.D. Khalaji, V. Tahmasebi, K. Gotoh, H. Ishida, Synthesis, characterization and crystal structures of new bidentate Schiff base ligand and its vanadium(IV) complex: The catalytic activity of vanadyl complex in epoxidation of alkenes, *Polyhedron* 31 (2012) 265–271; (c) G. Grivani, G. Bruno, H.A. Rudbari, A.D. Khalaji, P.A. Pourteimouri, Synthesis, characterization and crystal structure determination of a new oxovanadium(IV) Schiff base complex: The catalytic activity in the epoxidation of cyclooctene, *Inorg. Chem. Commun.* 18 (2012) 15–20.
- [50] C.D. Nunes, P.D. Vaz, V. Felix, L.F. Veiros, T. Moniz, M. Rangel, S. Realista, A.C. Mourato, Calhorda, Vanadyl cationic complexes as catalysts in olefin oxidation, *Dalton Trans* 44 (2015) 5125–5138.
- [51] P. Adao, J.C. Pessoa, R.T. Henriques, M.L. Kuznetsov, F. Avecilla, M.R. Maurya, U. Kumar, I. Correia, Synthesis, Characterization, and Application of Vanadium-Salan Complexes in Oxygen Transfer Reactions, *Inorg. Chem.* 48 (2009) 3542–3561.
- [52] M.R. Maurya, B. Mengesha, B. Uprety, N. Jangra, R. Tomara, F. Avecilla, Oxygen atom transfer between DMSO and benzoin catalyzed by cis-dioxidomolybdenum (VI) complexes of tetradentate Mannich bases, *New J. Chem.* 42 (2018) 6225–6235.
- [53] T. Joseph, D. Srinivas, C.S. Gopinath, S.B. Halligudi, Spectroscopic and Catalytic Activity Studies of VO(Saloph) Complexes Encapsulated in Zeolite-Y and Al-M-CM-41 Molecular Sieves, *Catal. Lett.* 83 (2002) 209–214.
- [54] L.M.D.R.S. Martins, A.J.L. Pombeiro, Tris(pyrazol-1-yl)methane metal complexes for catalytic mild oxidative functionalizations of alkanes, alkenes and ketones, *Coord. Chem. Rev.* 265 (2014) 74–88.
- [55] S. Huber, M. Cokoja, F.E. Kühn, Historical landmarks of the application of molecular transition metal catalysts for olefin epoxidation, *J. Organomet. Chem.* 751 (2014) 25–32.
- [56] J.J. Plata, L.C. Pacheco, E.R. Remesal, M.O. Masa, L. Vega, A.M. Márquez, J.A. Odriozola, J.F. Sanz, Analysis of the variables that modify the robustness of Ti-SiO<sub>2</sub> catalysts for alkene epoxidation: Role of silylation, deactivation and potential solution, *Mol. Catal.* 459 (2018) 55–60.
- [57] V. Conte, A. Coletti, B. Floris, G. Licini, C. Zonta, Mechanistic aspects of vanadium catalysed oxidations with peroxides, *Coord. Chem. Rev.* 255 (2011) 2165–2177.
- [58] A.D.M. Mohamad, E.R. El-Shrkawy, M.F.I. Al-Hussein, M.S.S. Adam, Water-soluble Cu(II)-complexes of Schiff base amino acid derivatives as biological reagents and sufficient catalysts for oxidation reactions, *J. Taiwan Inst. Chem. Eng.* 113 (2020) 27–45.
- [59] N.M.R. Martins, K.T. Mahmudov, M.F.C.G. da Silva, L.M.D.R.S. Martins, A.J.L. Pombeiro, Copper (II) and iron (III) complexes with arylhydrazone of ethyl 2-cyanoacetate or formazan ligands as catalysts for oxidation of alcohols, *New J. Chem.* 40 (2016) 10071.
- [60] L.H. Abdel-Rahman, A.M. Abu-Dief, M.S.S. Adam, S.K. Hamdan, Some new nano-sized mononuclear Cu(II) Schiff base complexes: design, characterization, molecular modeling and catalytic potentials in benzyl alcohol oxidation, *Catal. Lett.* 146 (2016) 1373–1396.
- [61] E. Steves, S.S. Stahl, Copper(I)/ABNO-Catalyzed Aerobic Alcohol Oxidation: Alleviating Steric and Electronic Constraints of Cu/TEMPO Catalyst Systems, *J. Am. Chem. Soc.* 135 (2013) 15742–15745.
- [62] M.S.S. Adam, Catalytic potentials of homodioxo-bimetallic dihydrazone complexes of uranium and molybdenum in a homogeneous oxidation of alkenes, *Monatsh. Chem.* 146 (2015) 1823–1836.
- [63] L.P. de Carvalho, K. F.Silva, L.L. dos Santos, M.V.P. dos Santos, J.A.B. da Silva, R.L. Longo, Chemoselective oxidation of unsaturated organosulfur, selenium and phosphorus compounds by molybdenum oxodiperoxo complexes: A computational investigation, *Inorg. Chim. Acta* 467 (2017) 351–357.
- [64] M. Morad, T.M. Habeebullah, I. Althagafi, B.H. Asghar, A.A. Bayazeed, T.M. Bawazeer, A.M. Al-Solimiy, N. El-Metwaly, Copper-acetanilide complexes: synthesis, characterization, crystal structure, computational analysis and their application as heterogeneous catalysts for biodiesel synthesis, *Res. Chem. Intermed.* 46 (2020) 4543–4562.
- [65] R. Shah, H. Katouah, A.A. Sedayo, M. Abualnaja, M.M. Aljohani, F. Saad, R. Zaky, N.M. El-Metwaly, Practical and computational studies on novel Schiff base complexes derived from green synthesis approach: Conductometry as well as *in-vitro* screening supported by *in-silico* study, *J. Mol. Liq.* 219 (2020) 114116.
- [66] A.S. Al-Wasidi, N.M. Al-Jafshar, A.M. Al-Anazi, M.S. Refat, N.M. El-Metwaly, H.K. Ibrahim, W. Abd El-Fattah, A.M. Naglah, M.A. Al-Omar, A. Kalmouch, In Methanolic Solvent Synthesis of New Mn<sup>II</sup>, Co<sup>II</sup>, Ni<sup>II</sup> and Cu<sup>II</sup> Schiff Base of Aromatic β Amino Acids: Spectroscopic, Thermal, Molecular Docking and Antimicrobial Studies, *Sci. Adv. Mater* 12 (2020) 1137–1148.
- [67] S.Y. Al-nami, E. Aljuhani, I. Althagafi, H.M. Abumelha, T.M. Bawazeer, A.M. Al-Solimiy, Z.A. Al-Ahmed, F. Al-Zahrani, N. El-Metwaly, Synthesis and Characterization for New Nanometer Cu(II) Complexes, Conformational Study and Molecular Docking Approach Compatible with Promising in Vitro Screening, *Arab. J. Sci. Eng.* DOI (2000), doi:10.1007/s13369-020-04814-x.
- [68] F. Alkhatib, H. Hameed, A. Sayqal, A.A. Bayazeed, S. Alzahrani, Z.A. Al-Ahmed, R. Zaky, N.M. El-Metwaly, Green-synthesis and characterization for new Schiff-base complexes; spectroscopy, conductometry, Hirshfeld properties and biological assay enhanced by in-silico study, *Arab. J. Chem.* 13 (2020) 6327–6340.